Quaternary Science Reviews 330 (2024) 108558

Contents lists available at ScienceDirect

Quaternary Science Reviews

journal homepage: www.elsevier.com/locate/quascirev

At an important tephrostratigraphic crossroads: cryptotephra in Late Glacial to Early Holocene lake sediments from the Carpathian Mountains, Romania

R.J. Kearney [a,b,*], P.G. Albert [a,c], R.A. Staff [a,d], E.K. Magyari [e], I. Pál [e], D. Veres [f,**], C.S. Lane [g], A. McGuire [g,h], C. Bronk Ramsey [a]

[a] Research Laboratory for Archaeology and the History of Art, School of Archaeology, University of Oxford, 1 South Parks Road, Oxford, UK
[b] Climate Dynamics and Landscape Evolution, GFZ Research Centre for Geoscience, Telegrafenberg, Potsdam, Germany
[c] Department of Geography, College of Science, Swansea, UK
[d] Scottish Universities Environmental Research Centre, University of Glasgow, Rankine Avenue, East Kilbride, South Lanarkshire, UK
[e] Eötvös Lóránd University, HUN-REN-MTM-ELTE Research Group for Palaeontology, Department of Environmental and Landscape Geography, Pázmány P. stny. 1/C, Budapest, Hungary
[f] Romanian Academy, Institute of Speleology, Clinicilor, Cluj-Napoca, Romania
[g] Department of Geography, University of Cambridge, Cambridge, UK
[h] School of Earth and Environment, Faculty of Environment, University of Leeds, Leeds, UK

ARTICLE INFO

Handling Editor: Giovanni Zanchetta

Keywords:
Tephrochronology
Cryptotephra
Tephrostratigraphy
Carpathian Mountains

ABSTRACT

Understanding the temporal and spatial environmental response to past climate change during the Last Glacial-Interglacial Transition (LGIT, 16-8 ka) across Europe relies on precise chronologies for palaeoenvironmental records. Tephra layers (volcanic ash) are a powerful chronological tool to synchronise disparate records across the continent. Yet, some regions remain overlooked in terms of cryptotephra investigations. Building on earlier work at the same sites, we present the first complete LGIT high-resolution cryptotephra investigation of two lake records in the Carpathian Mountains in Romania, Lake Brazi and Lake Lia. Numerous volcanic glass shards have been recognised as originating from various volcanic regions, including: Iceland (Katla, Askja, and Torfajokull), Italy (Campi Flegrei, Ischia, Lipari, and Pantelleria), and central Anatolia (Acigol and Ericyes). In total, four distinct tephra horizons have now been identified in these records: 1) an LGIT Lipari tephra (11,515–12,885 cal BP, 95.4% range); 2) Askja-S (11,070–10,720 cal BP, 95.4% range); 3) an Early Holocene Lipari tephra, (12,590–10,845 cal BP, 95.4% range) and; 4) an Early Holocene Ischia tephra (11,120–10,740 cal BP, 95.4% range). The use of trace element analysis on selected cryptotephra layers provided additional important information in identifying volcanic source and facilitating correlations. These tephra layers, along with numerous other discrete cryptotephra layers, offer promise as significant future isochrons for comprehending the spatial and temporal fluctuations in past climate change throughout Europe and the Mediterranean area. This research has emphasized the significance of the Carpathian region in expanding the European and Mediterranean tephra lattice and establishing it as a keystone area within the framework.

1. Introduction

Investigating the spatial and temporal environmental response to past abrupt climatic oscillations requires palaeoenvironmental records to have independent and precise chronologies (Björck et al., 1998; Lowe et al., 2008). The Late Glacial to Interglacial transition (LGIT, c.16-8 ka) was a period that experienced several abrupt climatic changes on centennial to decadal timescales, observed and dated in palaeoenvironmental records across Europe (e.g. Clark et al., 2001; Wohlfarth et al., 2006; Steffensen et al., 2008; Magyari et al., 2012; Rasmussen et al., 2014). Yet, challenges remain when trying to understand the timing and propagation of environmental responses to rapid climatic

* Corresponding author current address. Climate Dynamics and Landscape Evolution, GFZ Research Centre for Geoscience, Telegrafenberg, Potsdam, Germany.
** Corresponding author. Romanian Academy, Insitute of Speleology, Clinicilor, Cluj-Napoca, Romania
E-mail address: rkearney@gfz-potsdam.de (R.J. Kearney).

https://doi.org/10.1016/j.quascirev.2024.108558
Received 17 November 2023; Received in revised form 16 February 2024; Accepted 18 February 2024
Available online 20 March 2024

oscillations. Despite progress in geochronological methods, large dating uncertainties and the use of wiggle-matching or 'tuning' of disparate records continue to limit our ability to fully investigate assumptions of climatic (a)synchroneity between regions (e.g. Blaauw, 2012; Brauer et al., 2014; Bronk Ramsey et al., 2014).

The identification of distal volcanic ash (tephra) preserved in a range of climatic archives, such as ice cores (e.g. Cook et al., 2018), marine (e.g. Albert et al., 2015), and terrestrial (e.g. Lane et al., 2013) sedimentary records, has provided a powerful tool to precisely date (tephrochronology) and correlate (tephrostratigraphy) important environmental records together (e.g. Lowe, 2011; Davies, 2015). The development of specific laboratory methods, including the application of density separation (Turney, 1998), has allowed the detection of cryptotephra (non-visible) horizons within disparate palaeoenvironmental records to be made (e.g. van der Bilt et al., 2017; Pyne-O'Donnell and Jensen, 2020). Where well-characterised and widespread tephra marker layers are found in numerous palaeoenvironmental records within a region, a tephrostratigraphic framework or lattice can be established and expanded between regions (Bronk Ramsey et al., 2015; Lowe et al., 2015). This facilitates precise temporal integration of important palaeoenvironmental records across vast distances, providing insight into the temporal and spatial complexities of abrupt climatic events during the LGIT (e.g. Lane et al., 2013; Muschiello and Wohlfarth, 2015; Wohlfarth et al., 2018; Reinig et al., 2021).

Numerous European records have undergone cryptotephra investigations, particularly in northern and western Europe during the LGIT (e.g. Lowe et al., 2015; Timms et al., 2018). Yet, regions such as Central Eastern Europe, particularly Romania, have been largely overlooked for cryptotephra studies until now. This limits important continental-scale tephrostratigraphic frameworks from being developed. Previous tephra investigations have instead focused on visible volcanic ash layers in a range of sedimentary records across Romania, providing correlations to Mediterranean sources, as well as the Carpathian volcano, Ciomadul (e.g. Veres et al., 2013; Karátson et al., 2016; Obreht et al., 2017). The first cryptotephra investigation from sites in Romania undertaken by Kearney et al. (2018) highlighted the significant potential of the region in extending the European tephrostratigraphic framework with the successful identification of the ultra-distal Askja-S tephra from Askja Volcano, Iceland, dated to 10,824 ± 97 cal BP (2σ, Kearney et al., 2018). Further potential for Romania to provide a crucial tephrostratigraphic connection results from the close location of multiple volcanic fields that have been active throughout the Late Quaternary (Fig. 1), and being at the convergence of three major air masses, the Atlantic, the Mediterranean and the Siberian High (Haliuc et al., 2017; Longman et al., 2017a, 2017b; Obreht et al., 2017).

Here, we present the first complete LGIT cryptotephra investigation from two lacustrine palaeoenvironmental records in Romania, Lake Lia and Lake Brazi, located in the Southern Carpathian Mountains. The findings from this investigation provide a crucial connection between palaeoenvironmental records and volcanic regions within Europe and beyond.

2. Regional setting

The Retezat Mountains are located in southern Romania and form the western massif of the Southern Carpathian Mountains (Fig. 1). During the Last Glacial Maximum, the area underwent extensive glaciation (Urdea, 2004; Reuther et al., 2007; Ruszkiczay-Rüdiger et al., 2016). The retreat of glacial ice since the Last Glacial period resulted in 58 permanent glacial lakes (Jancsik, 2001). In the Galesul valley, two glacial lakes, Lake Brazi and Lake Lia, were selected for cryptotephra investigations. Both lakes were cored as part of the PROLONG project ('Providing long environmental records of Late Quaternary climatic oscillations in the Retezat Mountains', Magyari et al., 2018). The sediments retrieved from each lake have undergone high-resolution palaeoenvironmental investigations using numerous different proxies such as pollen, chironomids and diatoms (e.g. Magyari et al., 2009; Magyari et al., 2012; Pál et al., 2018). The results highlighted the importance of

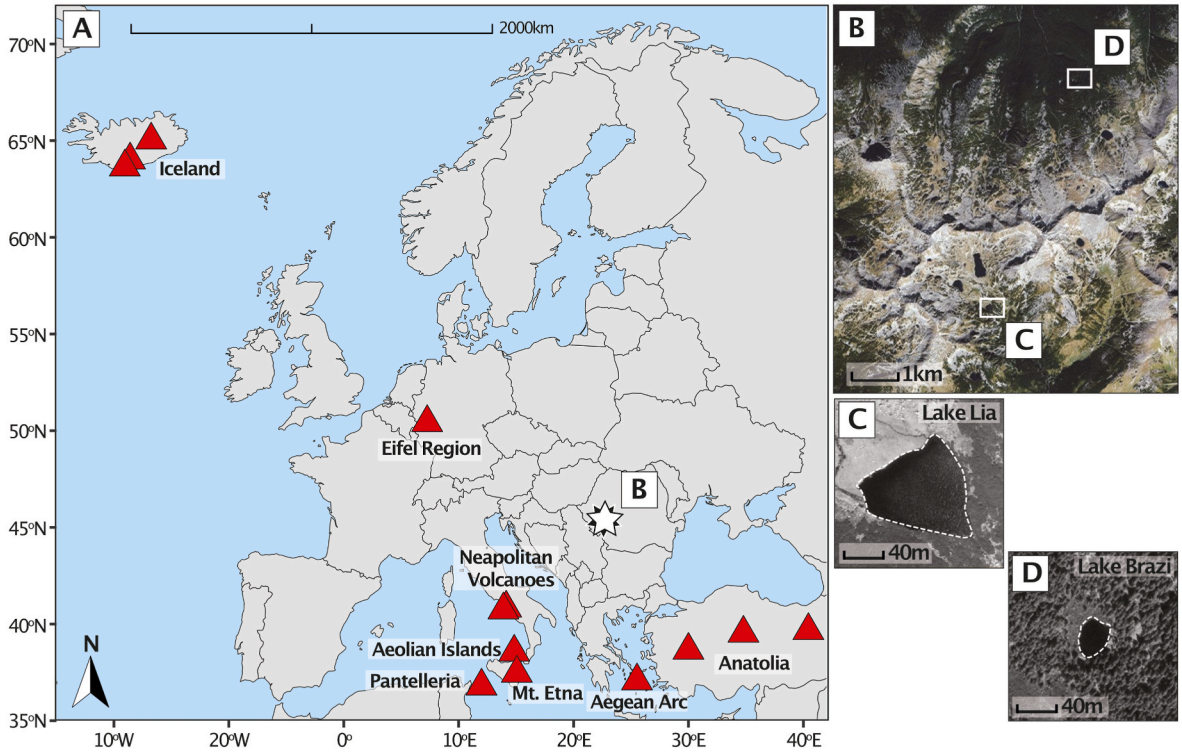

Fig. 1. ***A)*** *Map of Europe showing the proximity of selected volcanic centres that were known to be active during the LGIT period. The Neapolitan Volcanoes here refers to Campi Flegrei, Ischia and Vesuvius. The star indicates the location of Lakes Lia and Brazi.* ***B)*** *Location of Lake Lia* ***(C)*** *and Lake Brazi* ***(D)*** *in the Retezat Mountains (adapted from* Kearney et al., 2018 with satellite images for B-D using Google Earth Pro application (version 7.3.6, 2023) with data from CNES/Airbus.

this region in fully understanding environmental responses to past climatic change during the LGIT period (Pál et al., 2018). Both sites have chronologies provided by radiocarbon dating (Magyari et al., 2009, 2012; Hubay et al., 2018; Pál et al., 2018) which indicate a rapid sedimentation rate, ideal for the preservation of tephra layers, particularly cryptotephra (e.g. Lane et al., 2014; Davies, 2015). By providing a detailed reconstruction of the cryptotephra record at both sites, the aim of this study is to refine their ages of these tephras to aid palaeoenvironmental comparisons between other sedimentary records in Europe.

2.1. Lake Lia (LIA, 45°21′7.3″ N, 22°52′27.0″ E, 1910 m a.s.l)

Lake Lia is located on the southern side of the mountain range (Fig. 1). It is a small (12,600 m^2), shallow glacial lake (0.8 m deep), with two inflow streams from higher altitude lakes, principally Lake Bucura, and one outflow stream (Magyari et al., 2018). In 2008, an 880 cm long sediment core (LIA-1) was taken close to the western shore with a modified Livingstone corer (Hubay et al., 2018). Several multi-proxy palaeoenvironmental studies are currently underway with a chronology provided by seventeen radiocarbon dates (Hubay et al., 2018) and the identification of the Askja-S cryptotephra isochron (Kearney et al., 2018). No visible tephra layers have been identified within the core.

2.2. Lake Brazi (TDB, 45°23′47″ N, 22°54′06″ E, 1740 m a.s.l.)

Lake Brazi (Taul dintre Brazi, TDB) is located on the northern flank of the mountain range (Fig. 1). The lake is a kettle hole feature with a shallow depth (1.1m max depth) and smaller surface area (5,000 m^2, Magyari et al., 2009; Hubay et al., 2018). The lake receives seasonal underground inflow along the northern side with additional water sources from rainfall and slope inwash (Magyari et al., 2018). It has a single outflow located on the southern shore (Fig. 1). A modified Livingstone piston corer was used to retrieve a 490 cm long sediment core in 2007 (Magyari et al., 2009). A chronology is provided by twenty-one radiocarbon dates (Hubay et al., 2018) along with the identification of the Askja-S tephra (Kearney et al., 2018). No visible tephra layers have been identified within the core.

3. Material and methods

3.1. Cryptotephra sample preparation

Both cores were continuously sub-sampled at 5 cm resolution across the intervals relating to the LGIT (Magyari et al., 2009; Vincze et al., 2017). To reduce contamination issues, the sediment surface was cleaned as well as sampling instruments being cleaned between each sample. Where high cryptotephra shard concentrations were detected, the sediment was re-sampled at 1 cm resolution to better constrain the stratigraphic position of the shard count peaks. Glass shards were concentrated following a density separation procedure modified slightly from Turney (1998) and Blockley et al. (2005). Samples with high organic matter (peat) were combusted at 550 °C. Carbonates were subsequently removed by adding 10% HCl to each sample. The remaining residue was then sieved at 80 μm and 15 μm (instead of 80 μm and 25 μm) to further remove organic and minerogenic material. The retained sample then underwent density separation at 1.95–2.55 g cm^{-3}. Blank samples also went underwent the same laboratory treatment as these samples to rule out potential contamination. This extracted residue was then mounted on microscope slides using Canada balsam. A high-powered, polarizing optical microscope was used to identify and count the volcanic glass shards for each sample with shard concentrations given as the number of shards per gram of dry weight sediment. The individual tephra layers are named according to the site/core name and their respective depth (i.e. LIA-603 cm, TDB-564 cm).

3.2. Geochemical analysis

At depths where peaks in glass shard concentrations were observed, new samples were extracted from the cores and prepared for geochemical analysis as above, although without ashing, to avoid geochemical alteration due to high temperatures (Blockley et al., 2005). Individual glass shards were picked from extracted residues on a well-slide, using a micromanipulator under high-power microscopy, and mounted onto an epoxy resin stub (Lane et al., 2014). Each stub was sealed with resin and hand sectioned to expose a flat surface of the glass shards, which was then carbon-coated prior to electron probe microanalysis.

3.2.1. Major and minor element composition analysis

Individual glass shards were measured for major and minor element compositions using a JEOL-8600 wavelength-dispersive electron microprobe (WDS-EPMA) at the Research Laboratory for Archaeology and History of Art (RLAHA), University of Oxford using a 15 kV accelerated voltage, 6 nA beam current and 5–10 μm diameter beam. The probe was calibrated using a collection of mineral standards with the PAP absorption correction method for quantification. Peak counting times were 12s Na, 40s Mn, 50s Cl, 60 s P and 30s for all other elements. The MPI-DING reference glasses (ATHO-G, GOR132/5. St/Hs6/80-g) were used to assess the accuracy and precision of the analyses (Jochum et al., 2006).

All the data with analytical totals <92 wt% were removed. The major and minor element data was normalised (100%) on a volatile-free basis to allow comparisons and to account for hydration.

3.2.2. Trace element composition analysis

Analyses of specific samples were performed using an Agilent 8900 triple quadrupole ICP-MS (ICP-QQQ) coupled to a Resonetics 193 nm ArF excimer laser-ablation system housed in the Department of Earth Sciences, Royal Holloway, University of London. A spot size of 20 μm was selected due to the small shard sizes. A repetition rate of 5Hz with a count time of 40s on the sample with 40s gas blank was implemented. Instrument calibration was undertaken, analysing NIST612, with ^{29}Si (determined by EPMA) as the internal standard. The MPI-DING reference glasses (StHs6/80-G, ATHO-G, GOR132-G) were analysed alongside unknowns to monitor analytical accuracy (Jochum et al., 2006). Full analytical methods and data reduction methods are outlined by Tomlinson et al. (2010). The full geochemical dataset can be seen in Supplementary Table S1.

3.3. Age depth modelling

A Bayesian age-depth model for Lake Lia and Brazi was constructed using previously published radiocarbon dates by Hubay et al. (2018) and OxCal version 4.4 (Bronk Ramsey, 2021), applying the updated IntCal20 calibration curve (Reimer et al., 2020). A total of seventeen radiocarbon ages for Lake Lia and twenty for Lake Brazi were incorporated into the model (Hubay et al., 2018). However, one radiocarbon age from each of the lakes was subsequently removed due to being erroneously young for their stratigraphic positions, DeA-3247 for Lia and Poz-26113 for Brazi. The age model was constructed using '*P_Sequence*' deposition models for both sites with a variable *k* parameter to allow flexibility in sedimentation rate within the models (Bronk Ramsey, 2008; Bronk Ramsey and Lee, 2013). A 'General' *Outlier_Model* with 5% prior probability that individual radiocarbon dates were statistical outliers was applied to the individual radiocarbon dates (Bronk Ramsey, 2009). As a result of the previous identification of the Askja-S tephra layer, and with the assumption that the tephra layers are synchronous between depositional records (Lowe, 2011), cross-referencing was applied to the depths where the Askja-S has been identified. The ages presented in the remainder of this paper are all derived from this composite age model, and are presented at 95.4% (~2σ) highest probability density, unless stated.

4. Results

4.1. Tephrostratigraphy

Within Lake Lia, eighteen cryptotephra peaks were identified at high resolution (1 cm) through the LGIT part of the LIA-1 core and geochemically investigated (Fig. 2). Certain intervals of the core contained no glass shards. The peak shard concentrations ranged from 38 shards/g^{-1} (LIA_713) to 908 shards/g^{-1} (LIA_603). The lower depths of the core contain lower shard counts, with higher concentrations observed towards the top.

In Lake Brazi tephra glass shards appear, in varied concentration, within all samples that were investigated from the LGIT record of TDB-1. A total of twelve cryptotephra horizons were identified based on having higher shard concentration compared to the preceding sample or where no shards were present in the sample below (Fig. 2). The highest peak in shard concentration, at 564 cm depth, with 1,135 shards/g^{-1}, appears as a sudden increase from previous samples, none of which contain greater than 400 shards/g^{-1}. Due to the constant shard background, other peaks were less clearly defined in the record (e.g. TDB_540 and TDB_541).

4.2. Glass chemistry compositions

The geochemical results for the individual glass shards from the identified cryptotephra peaks in both lakes are presented in Fig. 3. For simplicity, and due to the high number of analyses, the variations in major and minor elemental glass composition from both lakes were assigned to two broad geochemical groups that correspond to differences in SiO_2 values: 1) rhyolitic and 2) trachytic (Table 1, Table 2 and Fig. 4). Within these groups, there are further sub-divisions reflecting differing heterogeneous compositions. Many of the cryptotephra horizons from Lake Lia and Brazi contain glass shards that belong to several geochemical groups and which may be associated with reworking within the sediment profile (see Section 5.1).

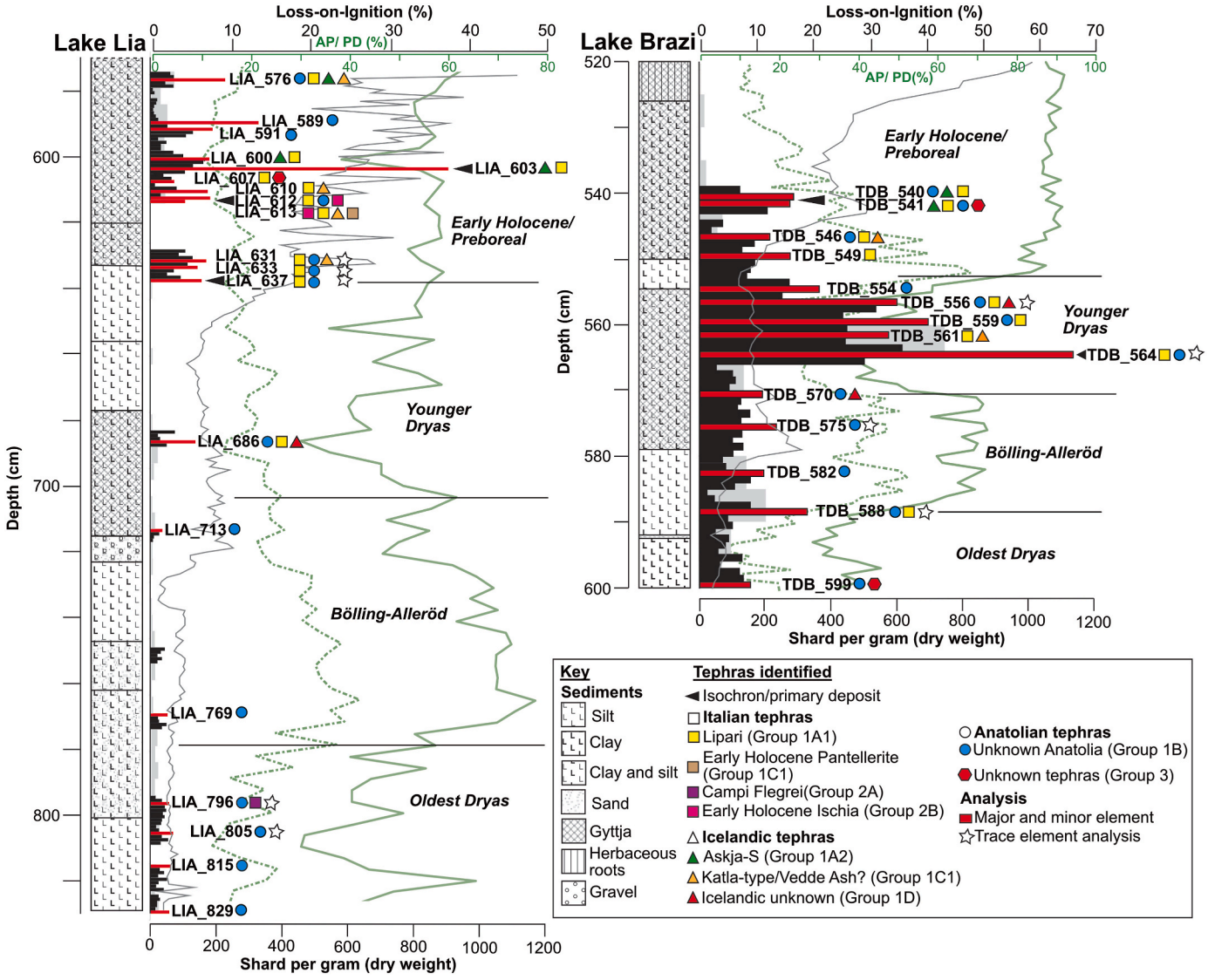

Fig. 2. *Shard concentration profile along with lithostratigraphy and loss-on-ignition for Lake Lia and Lake Brazi for the Late Glacial and Early Holocene period. Low resolution shard counts (5 cm) are indicated with light grey and higher resolution shard counts (1 cm) in black. Red indicates shard peaks that underwent major and minor element analysis. Symbols indicate tephra geochemical groups, assigned to their volcanic source, as described in section 4. Order of these symbols (L-R) indicates relative proportions (high-low) of each compositional population in each layer (see Table 3 for more information). Palaeoecological zones and percentage arboreal pollen (AP, solid green line) and Pinus Dyploxylon (PD, dotted green line) presented according to information from* Magyari et al. (2009a, 2018) and Vincze et al. (2017). For further explanation of the pollen stratigraphic zonation see Magyari et al. (2018).

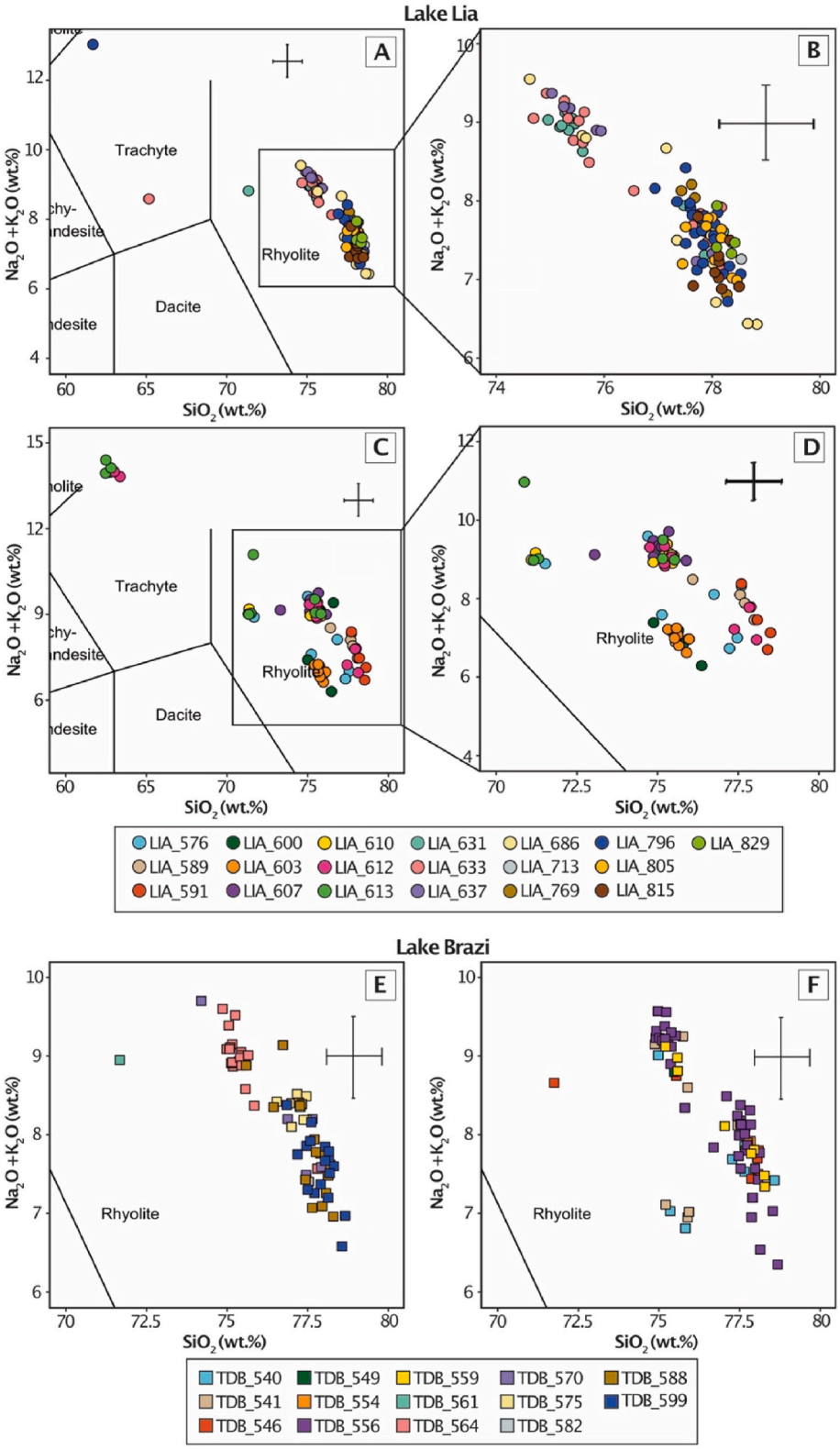

Fig. 3. Total alkali versus silica (TAS) classification plots showing the glass compositions of analysed cryptotephra samples from the following depths in Lake Lia (A–B: LIA_829-LIA_631; C–D: LIA_613-LIA_576 [cm]) and Lake Brazi (E–F) (Le Bas et al., 1986). Error bars represent 2 standard deviations of repeat analysis of the MPI-DING StHs6/80-G glass standard.

Table 1
Summary information for Lake Lia tephra groups.

Depth	LIA_829		LIA_815		LIA_805		LIA_796				LIA_769		LIA_713		LIA_686			
Group	1		1		1		1		2		1		1		1		1	
Sub-group	B		B		B		B		A		B		B		A1		B	
Shards	n = 5		n = 9		n = 13		n = 27		n = 1		n = 4		n = 1		n = 2		n = 9	
Major	Mean	±1sd	Mean	±1sd	Mean	±1sd	Mean	±1sd	Mean	±1sd	Mean	±1sd	Mean	±1sd	Mean	±1sd	Mean	±1sd
SiO2	78.24	0.18	78.09	0.26	78.07	0.33	77.87	0.41	61.69	n/a	77.75	0.36	78.54	n/a	75.62	0.05	78.03	0.53
TiO2	0.07	0.05	0.09	0.05	0.07	0.05	0.07	0.04	0.46	n/a	0.04	0.02	0.05	n/a	0.07	0.06	0.08	0.03
Al2O3	12.56	0.34	12.50	0.16	12.52	0.24	12.55	0.22	18.54	n/a	12.51	0.09	12.46	n/a	12.98	0.10	12.51	0.16
FeOt	0.84	0.21	1.08	0.22	0.99	0.17	0.94	0.20	2.91	n/a	0.94	0.13	0.86	n/a	1.38	0.04	1.02	0.13
MnO	0.00	0.01	0.07	0.07	0.05	0.05	0.05	0.04	0.01	n/a	0.07	0.05	0.00	n/a	0.05	0.01	0.03	0.03
MgO	0.02	0.02	0.06	0.03	0.04	0.03	0.05	0.02	0.46	n/a	0.06	0.04	0.07	n/a	0.02	0.02	0.06	0.05
CaO	0.62	0.07	0.78	0.17	0.74	0.17	0.07	0.04	2.16	n/a	0.70	0.22	0.60	n/a	0.68	0.04	0.79	0.22
Na2O	4.07	0.45	4.01	0.35	3.75	0.44	3.72	0.80	4.53	n/a	4.08	0.52	3.63	n/a	3.92	0.16	3.77	0.40
K2O	3.47	0.64	3.17	0.51	3.62	0.62	3.86	1.01	8.50	n/a	3.72	0.61	3.63	n/a	4.89	0.14	3.53	0.82
Total	93.65	0.70	93.21	0.62	93.13	0.90	94.33	1.26	97.76	n/a	94.42	1.24	93.20	n/a	95.77	0.01	93.86	1.63

Depth	LIA_686		LIA_637				LIA_633								LIA_631			
Group	1		1		1		1		1		3		3		1		1	
Sub-group	D		A1		B		A1		B						A1		B	
Shards	n = 1		n = 6		n = 3		n = 12		n = 5		n = 1		n = 1		n = 8		n = 6	
Major	Mean	±1sd	Mean	±1sd	Mean	±1sd	Mean	±1sd	Mean	±1sd	Mean	±1sd	Mean	±1sd	Mean	±1sd	Mean	±1sd
SiO2	74.62	n/a	75.56	0.40	77.94	0.20	75.57	0.60	77.93	0.23	65.17	n/a	76.55	n/a	75.30	0.20	77.86	0.23
TiO2	0.21	n/a	0.09	0.05	0.07	0.03	0.08	0.03	0.02	0.03	1.01	n/a	0.04	n/a	0.08	0.04	0.08	0.03
Al2O3	11.76	n/a	12.56	0.56	12.80	0.13	12.90	0.19	12.82	0.16	14.10	n/a	12.79	n/a	12.98	0.21	12.43	0.26
FeOt	2.82	n/a	1.52	0.47	0.93	0.10	1.32	0.32	0.86	0.13	6.48	n/a	1.00	n/a	1.46	0.12	0.97	0.14
MnO	0.23	n/a	0.08	0.06	0.00	0.00	0.10	0.06	0.05	0.05	0.29	n/a	0.06	n/a	0.06	0.05	0.04	0.04
MgO	0.00	n/a	0.02	0.02	0.06	0.01	0.04	0.03	0.01	0.01	0.95	n/a	0.11	n/a	0.02	0.02	0.04	0.03
CaO	0.35	n/a	0.61	0.23	0.77	0.24	0.74	0.14	0.56	0.04	2.96	n/a	1.14	n/a	0.73	0.07	0.81	0.24
Na2O	4.93	n/a	4.17	0.42	3.98	0.29	3.76	0.49	4.11	0.24	5.95	n/a	2.52	n/a	3.99	0.18	3.98	0.12
K2O	4.62	n/a	4.99	0.23	3.31	0.32	5.13	0.20	3.50	0.16	2.64	n/a	5.60	n/a	4.96	0.17	3.65	0.31
Total	95.87	n/a	94.80	0.79	92.95	0.67	95.53	0.94	93.80	0.85	94.17	n/a	95.99	n/a	95.83	1.48	93.88	1.70

Depth	LIA_631 (cont.)		LIA_613								LIA_612						LIA_610	
Group	1		1		1		1		2		1		1		2		1	
Sub-group	C1		A1		A1		C2		B		A1		B		B		A1	
Shards	n = 1		n = 3		n = 6		n = 1		n = 3		n = 5		n = 4		n = 3		n = 6	
Major	Mean	±1sd	Mean	±1sd	Mean	±1sd	Mean	±1sd	Mean	±1sd	Mean	±1sd	Mean	±1sd	Mean	±1sd	Mean	±1sd
SiO2	71.36	n/a	75.29	0.21	71.24	0.06	70.87	n/a	62.10	0.22	75.17	0.25	77.80	0.29	62.57	0.34	75.28	0.22
TiO2	0.17	n/a	0.06	0.02	0.29	0.02	0.34	n/a	0.55	0.03	0.09	0.05	0.11	0.12	0.49	0.03	0.09	0.02
Al2O3	13.50	n/a	12.88	0.19	13.65	0.14	7.58	n/a	18.32	0.30	12.92	0.17	12.95	0.70	18.30	0.10	12.89	0.15
FeOt	4.04	n/a	1.43	0.07	3.83	0.14	8.40	n/a	2.51	0.12	1.49	0.09	0.83	0.04	2.43	0.11	1.36	0.14
MnO	0.28	n/a	0.05	0.06	0.16	0.11	0.30	n/a	0.25	0.03	0.06	0.03	0.03	0.03	0.20	0.05	0.09	0.05
MgO	0.23	n/a	0.02	0.02	0.22	0.02	0.04	n/a	0.31	0.02	0.04	0.01	0.06	0.07	0.26	0.04	0.04	0.03
CaO	1.43	n/a	0.72	0.08	1.36	0.07	0.45	n/a	1.13	0.07	0.72	0.06	0.68	0.31	1.18	0.02	0.75	0.07
Na2O	5.17	n/a	4.10	0.19	5.43	0.12	6.79	n/a	7.76	0.33	4.06	0.27	4.53	0.45	7.35	0.13	4.11	0.20
K2O	4.04	n/a	5.07	0.12	3.57	0.15	4.18	n/a	6.28	0.12	5.02	0.10	2.90	0.80	6.47	0.10	4.99	0.16
Total	98.45	n/a	93.84	0.75	98.62	0.28	93.02	n/a	97.92	3.15	95.59	0.57	94.74	1.46	97.85	1.03	95.32	0.41

Depth	LIA_610 (cont.)		LIA_607				LIA_603				LIA_600						LIA_591	
Group	1		1		3		1		1		1		1		3		1	
Sub-group	C1		A1				A1		A2		A1		A2				B	
Shards	n = 2		n = 7		n = 1		n = 1		n = 9		n = 1		n = 7		n = 1		n = 4	
Major	Mean	±1sd	Mean	±1sd	Mean	±1sd	Mean	±1sd	Mean	±1sd	Mean	±1sd	Mean	±1sd	Mean	±1sd	Mean	±1sd
SiO2	71.15	0.10	75.15	0.37	73.05	n/a	75.51	n/a	75.64	0.20	75.03	n/a	75.67	0.46	76.33	n/a	78.15	0.41

(*continued on next page*)

Table 1 (*continued*)

Depth	LIA_610 (cont.)		LIA_607			LIA_603			LIA_600				LIA_591		
TiO2	0.31	0.01	0.09	0.06	0.11	n/a	0.03	n/a	0.29	0.03	0.09	n/a	0.33	0.03	0.07	n/a	0.10	0.06
Al2O3	13.53	0.13	12.96	0.14	12.82	n/a	12.93	n/a	12.36	0.17	12.71	n/a	12.35	0.13	11.25	n/a	12.65	0.12
FeOt	3.94	0.00	1.34	0.22	3.62	n/a	1.30	n/a	2.62	0.13	1.50	n/a	2.54	0.13	2.37	n/a	0.84	0.30
MnO	0.12	0.03	0.04	0.05	0.15	n/a	0.02	n/a	0.11	0.04	0.00	n/a	0.08	0.03	0.12	n/a	0.04	0.04
MgO	0.20	0.00	0.03	0.02	0.02	n/a	0.04	n/a	0.25	0.02	0.07	n/a	0.25	0.04	11.25	n/a	0.04	0.04
CaO	1.41	0.01	0.68	0.06	0.77	n/a	0.69	n/a	1.61	0.06	0.81	n/a	1.67	0.02	0.15	n/a	0.62	0.08
Na2O	5.51	0.10	4.16	0.14	3.90	n/a	4.08	n/a	4.39	0.16	4.37	n/a	4.40	0.33	5.10	n/a	3.86	0.35
K2O	3.57	0.02	5.17	0.23	5.22	n/a	5.00	n/a	2.60	0.06	5.04	n/a	2.56	0.03	4.28	n/a	3.55	0.78
Total	95.18	2.36	93.80	0.66	94.94	n/a	95.55	n/a	98.80	0.82	93.69	n/a	96.89	1.74	94.93	n/a	95.54	1.63

Depth	LIA_589			LIA_576											
Group	1			1			1			1			1		
Sub-group	B			A1			A2			B			C1		
Shards	n = 4			n = 4			n = 2			n = 4			n = 1		
Major	Mean		±1sd	Mean		±1sd	Mean		±1sd	Mean		±1sd	Mean		±1sd
SiO2	77.34		0.85	75.07		0.31	75.46		0.46	77.26		0.38	71.52		n/a
TiO2	0.03		0.03	0.08		0.04	0.35		0.01	0.13		0.06	0.31		n/a
Al2O3	12.81		0.14	12.90		0.18	12.33		0.07	12.53		0.18	13.41		n/a
FeOt	0.96		0.21	1.51		0.12	2.50		0.12	1.29		0.47	3.84		n/a
MnO	0.08		0.02	0.04		0.03	0.13		0.05	0.07		0.03	0.18		n/a
MgO	0.03		0.04	0.04		0.01	0.25		0.01	0.07		0.05	0.25		n/a
CaO	0.57		0.04	0.71		0.03	1.64		0.04	0.99		0.32	1.39		n/a
Na2O	3.96		0.35	4.17		0.25	4.60		0.46	3.97		0.36	5.27		n/a
K2O	4.02		0.69	5.09		0.06	2.62		0.07	3.57		0.62	3.62		n/a
Total	92.91		1.39	95.76		1.14	96.64		1.13	93.23		0.74	98.41		n/a

4.2.1. *Group 1 rhyolitic tephras*

Throughout both Lia and Brazi, the majority of tephra layers contained glass shards of rhyolitic composition (Figs. 3 and 4). However, there are variations in the SiO_2 content, allowing broad sub-divisions into A-, B- and C-type tephra groupings.

4.2.1.1. Group 1A rhyolites with intermediate SiO_2 (75.0–76.5 wt%) content. Group 1A comprises of glass shards that are rhyolitic in composition with intermediate SiO_2 content (74.70–75.89 wt%). Further sub-division of this geochemical group can be made based upon K_2O and CaO content (Tables 1 and 2). Group 1A1 tephra can be distinguished based upon higher K_2O content (4.79–5.61 wt%) associated with a HKCA (High-K calc-alkaline) affinity composition and lower CaO (<1.0 wt%) content (Fig. 4A and B). These clear shards are comprised of fluted, platy and cuspate morphologies, ranging from 20 to 100 μm in length. Glass shards with this chemical composition were identified in Lia at depths labelled LIA_686, 637, 633, 631, 613, 612, 610, 607, 603, 600, 576 and Brazi at TDB_588, 564, 559, 556, 549, 546, 541, 540 (cm). Trace element analysis was conducted on certain tephra shards (n = 16) associated with Group 1A1 (LIA_637, 633, 631, TDB_564, 566; Fig. 5). Normalised to primitive mantle, these glasses show depletions in Ba, Sr and Eu, consistent with K-feldspar fractionation (Fig. 5). These shards show enrichment in Light Rare Earth Elements (LREE) relative to Heavy Rare Earth Elements (HREE) (La/Yb = 6.5–10.2).

The second sub-divided group, Group 1A2, has lower K_2O (<3.0 wt %) and CaO content (1.5–1.7 wt%) compared to preceding group 1A1 (Fig. 4A and B). These shards have a colourless, fluted appearance with shard sizes ranging from 20 to 25 μm. Group 1A2 can be found in Lia at LIA_603, 600, 576 and Brazi at TDB_541, 540. This group has identified and reported previously by Kearney et al. (2018).

4.2.1.2. Group 1B rhyolites with high SiO_2 (>76 wt%) content. Group 1B has glass shards with high SiO_2 content (>76.0 wt%), with low CaO (<1.3 wt%) and FeO_t (<1.5 wt%) (Fig. 4D). Group 1B tephras have variations in K_2O (2.06–7.16 wt%), straddling the calc-alkaline and HKCA boundary. The clear shards' morphologies are mixed between platy, cuspate and fluted glass with shard sizes ranging from 20 to >100 μm. Trace element analysis was undertaken on these high-SiO_2 rhyolitic shards from both lakes (LIA_796, 637. TDB_588, 575, 556). Normalised to primitive mantle, these glass shards show LREE enrichment relative to the HREE (La/Yb = 7.3–30.9) with element concentrations of: Th 12.4–24.9 ppm, Rb 140.4–282.0 ppm, Y 5.2–40.9 ppm, and La 17.4–35.0 ppm. These glasses show a depletion in Nb and Ta with an enrichment in Th (Fig. 5), consistent with an origin from a subduction setting.

Glass shards with Group 1B compositions were identified in cryptotephra layers from Lia (LIA_829, 815, 805, 796, 769, 713, 686, 637, 633, 631, 612, 591, 589, 576) and in the majority of Brazi layers (TDB_599, 588, 582, 575, 570, 564, 559, 556, 554, 546, 541, 540 [cm]).

4.2.1.3. Group 1C rhyolites with low SiO_2 (<74 wt%) content. The glass shards of Group 1C are rhyolitic with lower in SiO_2 content and heterogenous compositions clearly originating from different volcanic sources, allowing further sub-division into Groups 1C1 and 1C2 reflecting lower and higher FeO_t distributions, respectively (Fig. 4E and F). Group 1C1 has 71.39–71.75 wt% SiO_2 content with 1.31–1.43 wt% CaO and 3.73–4.04 wt% FeO_t. Glass shards associated with this sub-group were identified in cryptotephra layers of Lake Lia (LIA_631, 610, 613 and 576 [cm]) and two layers in Lake Brazi (TDB_546 and 561 [cm]). A single shard associated with this sub-group underwent trace element analysis (LIA_631 [cm], Fig. 5). Trace element analysis normalised to primitive mantle shows enrichment in Rb, Th, Nb and Ta, indicative of anorogenic volcanic settings. The shard morphologies geochemically assigned to Group 1C1 are predominately platy, with some cuspate and fluted glass, with shard sizes ranging from 20 to 80 μm.

Table 2
Summary information for Lake Brazi tephra groups.

Depth	TDB_599				TDB_588				TDB_582		TDB_575		TDB_570		TDB_564			
Group	1		1		1		1		1		1		1		1		1	
Sub-group	B		D		A1		B		B		B		B		A1		B	
Shards	n = 16		n = 1		n = 1		n = 15		n = 1		n = 8		n = 5		n = 20		n = 1	
Major	Mean	±1sd	Mean	±1sd	Mean	±1sd	Mean	±1sd	Mean	±1sd	Mean	±1sd	Mean	±1sd	Mean	±1sd	Mean	±1sd
SiO2	77.95	0.82	76.85	n/a	75.59	n/a	77.60	1.08	77.53	n/a	77.16	0.62	77.47	0.88	75.29	0.25	77.80	n/a
TiO2	0.08	0.09	0.10	n/a	0.09	n/a	0.07	0.10	0.07	n/a	0.05	0.07	0.06	0.08	0.08	0.04	0.09	n/a
Al2O3	12.44	0.29	12.21	n/a	12.66	n/a	12.52	0.30	13.09	n/a	12.51	0.38	12.59	0.26	12.95	0.09	12.47	n/a
FeOt	0.96	0.33	1.04	n/a	1.54	n/a	0.94	0.46	1.12	n/a	0.81	0.56	0.98	0.71	1.43	0.11	1.12	n/a
MnO	0.04	0.11	0.10	n/a	0.14	n/a	0.03	0.06	0.02	n/a	0.03	0.07	0.06	0.16	0.09	0.04	0.11	n/a
MgO	0.05	0.08	0.11	n/a	0.02	n/a	0.06	0.08	0.03	n/a	0.04	0.06	0.05	0.05	0.02	0.02	0.04	n/a
CaO	0.80	0.43	1.09	n/a	0.79	n/a	0.83	0.53	0.63	n/a	0.89	0.38	0.77	0.21	0.70	0.05	0.65	n/a
Na2O	3.56	0.95	2.29	n/a	3.83	n/a	3.69	1.63	3.96	n/a	2.95	1.55	3.34	1.60	3.97	0.27	3.31	n/a
K2O	3.98	1.03	6.09	n/a	5.05	n/a	4.12	2.66	3.44	n/a	5.38	1.72	4.53	2.10	5.04	0.12	4.27	n/a
Total	93.71	2.15	93.81	n/a	96.17	n/a	93.32	1.73	94.67	n/a	94.03	1.89	93.59	3.50	95.29	1.09	94.00	n/a

Depth	TDB_561				TDB_559				TDB_556						TDB_554		TDB_549	
Group	1		1		1		1		1		1		3		1		1	
Sub-group	A1		C1		A1		B		A1		B				B		A1	
Shards	n = 1		n = 1		n = 5		n = 3		n = 14		n = 23		n = 1		n = 3		n = 1	
Major	Mean	±1sd	Mean	±1sd	Mean	±1sd	Mean	±1sd	Mean	±1sd	Mean	±1sd	Mean	±1sd	Mean	±1sd	Mean	±1sd
SiO2	75.36	n/a	71.67	n/a	77.88	1.01	75.45	0.43	75.23	0.50	77.79	0.72	76.69	n/a	77.75	0.18	75.47	n/a
TiO2	0.06	n/a	0.25	n/a	0.08	0.11	0.04	0.04	0.07	0.07	0.05	0.07	0.04	n/a	0.02	0.06	0.09	n/a
Al2O3	12.96	n/a	13.33	n/a	12.63	0.47	12.96	0.08	12.95	0.35	12.66	0.32	12.97	n/a	12.57	0.13	13.06	n/a
FeOt	1.44	n/a	3.78	n/a	0.80	0.23	1.35	0.03	1.37	0.21	0.90	0.32	1.29	n/a	0.81	0.04	1.43	n/a
MnO	0.05	n/a	0.15	n/a	0.09	0.11	0.07	0.12	0.06	0.06	0.06	0.10	0.11	n/a	0.10	0.11	0.10	n/a
MgO	0.00	n/a	0.21	n/a	0.05	0.09	0.05	0.04	0.03	0.03	0.03	0.06	0.02	n/a	0.03	0.05	0.04	n/a
CaO	0.75	n/a	1.42	n/a	0.61	0.08	0.69	0.09	0.72	0.18	0.66	0.32	0.93	n/a	0.60	0.10	0.66	n/a
Na2O	3.74	n/a	5.39	n/a	3.59	1.06	3.87	0.31	4.15	0.42	4.14	0.78	4.30	n/a	3.99	0.83	3.74	n/a
K2O	5.20	n/a	3.56	n/a	4.11	1.47	5.10	0.11	5.05	0.62	3.59	1.04	3.54	n/a	3.99	0.76	5.05	n/a
Total	95.18	n/a	95.74	n/a	94.19	2.99	94.98	3.25	94.09	2.23	93.18	1.38	93.31	n/a	93.65	0.41	96.25	n/a

Table 3
Summary information for each tephra layer from Lake Lia and Brazi.

Site	Depth code	Mean age ± 1σ (cal. BP)	Age range (2σ, cal. BP)	Pollen-stratigraphic zone	Source Volcano	Layer type	Tephra isochron
Lia	LIA_576	10,705 ± 85	10,875 - 10525	Early Holocene	Anatolian Unknown (36%), Lipari (36%), Askja (18%), Katla (10%)	Reworked	
	LIA_589	10,785 ± 85	11,005–10,655	Early Holocene	Anatolian Unknown (100%)	Reworked	
	LIA_591	10,800 ± 85	11,010–10,655	Early Holocene	Anatolian Unknown (100%)	Reworked	
	LIA_600	10,850 ± 90	11,045–10,710	Early Holocene	Askja (88%), Lipari (22%)	Reworked	
	LIA_603	**10,865 ± 90**	**11,070–10,720**	**Early Holocene**	Askja (90%), Lipari (10%)	**Primary**	**Askja-S**
	LIA_607	10,895 ± 110	11,075–10,730	Early Holocene	Lipari (88%), Unknown (22%)	Reworked	
	LIA_610	10,915 ± 120	11,090–10,730	Early Holocene	Lipari (75%), Katla (25%)	Reworked	
	LIA_612	10,930 ± 130	11,120-10740	Early Holocene	Lipari (42%), Anatolian Unknown (33%), Ischia (25%)	Reworked	
	LIA_612.5	**10,935 ± 130**	**11,120–10,740**	**Early Holocene**	**Ischia**	**Primary**	**Early Holocene Ischia**
	LIA_613	10,940 ± 135	11,120–10,745	Early Holocene	Lipari (33%), Ischia (33%), Katla (22%), Pantelleria (11%)	Reworked	
	LIA_631	11,335 ± 430	12,375–10,800	Early Holocene	Lipari (53%), Anatolian Unknown (40%), Katla (7%)	Reworked	
	LIA_633	11,415 ± 455	12,470–10,820	Early Holocene	Lipari (59%), Anatolian Unknown (29%), Unknown (12%)	Reworked	
	LIA_637	**11,565 ± 495**	**12,590- 10,845**	Early Holocene	**Lipari (63%),** Anatolian Unknown (37%)	**Early Holocene Lipari Isochron**	**Early Holocene Lipari**
	LIA_686	13,320 ± 210	14,265–13,110	Younger Dryas	Anatolian Unknown (75%), Lipari (22%), Icelandic Unknown (11%)	Reworked	
	LIA_713	13,875 ± 510	14,975–13,205	Bölling-Alleröd	Anatolian Unknown (100%)	Reworked	
	LIA_769	15,020 ± 875	16,830–13,575	Oldest Dryas	Anatolian Unknown (100%)	Reworked	
	LIA_796	15,575 ± 1020	17,670–13,855	Oldest Dryas	Anatolian Unknown (96%), Campi Flegrei (4%, 1 shard)	Reworked	
	LIA_805	15,760 ± 1110	17,955–13,960	Oldest Dryas	Anatolian Unknown (100%)	Reworked	
	LIA_815	16,250 ± 1180	18,670–14,255	Oldest Dryas	Anatolian Unknown (100%)	Reworked	
	LIA_829	16,250 ± 1180	18,670–14,255	Oldest Dryas	Anatolian Unknown (100%)	Reworked	
Brazi	TDB_540	10,850 ± 100	11,075–10,225	Early Holocene	Anatolian Unknown (36%), Askja (29%), Lipari (14%)	Reworked	
	TDB_540.5	**10,865 ± 90**	**11,070–10,720**	**Early Holocene**	**Askja-S**	**Askja-S Isochron**	**Askja-S**
	TDB_541	10,880 ± 95	11,075–10,730	Early Holocene	Askja (43%), Lipari (29%), Anatolian Unknown (14%), Unknown (14%)	Reworked	
	TDB_546	11,015 ± 140	11,290–10,770	Early Holocene	Anatolian Unknown (66%), Lipari (17%), Katla (17%)	Reworked	
	TDB_549	11,155 ± 195	11,550–10,805	Early Holocene	Lipari (100%, 1 shard)	Reworked	
	TDB_554	11,390 ± 205	11,795–10,980	Younger Dryas	Anatolian Unknown (100%)	Reworked	
	TDB_556	11,485 ± 185	11,845–11,135	Younger Dryas	Anatolian Unknown (62%), Lipari (35%), Icelandic Unknown (3%)	Reworked	
	TDB_559	11,745 ± 325	12,530–11,240	Younger Dryas	Anatolian Unknown (63%), Lipari (37%)	Reworked	
	TDB_561	11,960 ± 385	12,720–11,305	Younger Dryas	Lipari (50%), Katla (50%)	Reworked	Vedde Ash?
	TDB_564	**12,280 ± 395**	**12,885–11,515**	**Younger Dryas**	**Lipari (95%), Anatolian Unknown (5%)**	**LG Lipari Isochron**	**LG Lipari**
	TDB_570	12,885 ± 160	13,270–12,720	Bölling-Alleröd	Anatolian Unknown (80%), Icelandic Unknown (20%)	Reworked	
	TDB_575	13,215 ± 215	13,510–12,800	Bölling-Alleröd	Anatolian Unknown (100%)	Reworked	
	TDB_582	13,530 ± 195	13,990–13,305	Bölling-Alleröd	Anatolian Unknown (100%)	Reworked	
	TDB_588	13,700 ± 275	14,325–13,330	Oldest Dryas	Anatolian Unknown (94%), Lipari Unknown (6%)	Reworked	
	TDB_599	14,020 ± 385	14,850–13,420	Oldest Dryas	Anatolian Unknown (94%), Unknown (6%)	Reworked	

Group 1C2 contains only a single shard from LIA_613, comprised of 70.87 wt% SiO_2 with an HKCA affinity (4.18 wt% K_2O) and distinctly high FeO_t content (8.40 wt%) (Fig. 4E and F).

4.2.2. Group 2 trachytic tephras

The trachytic glass shard of Group 2 were only identified in Lake Lia. All these glasses are distinctly lower in SiO_2 (<65 wt%). The group can be sub-divided based upon alkali ratio (K_2O/Na_2O) into 2A- (high), 2B- (low) and 2C- (very low) type tephras (Fig. 4G and H).

4.2.2.1. Group 2A trachytic tephra with high alkali ratio. Group 2A consists of a single High-K trachytic glass shard (SiO_2 = 61.69 wt%; K_2O = 8.50 wt%) from LIA_796 [cm]. This shard also displays high Al_2O_3 (18.54 wt%), FeO_t (2.91 wt%) and CaO (2.16 wt%) with a high alkali ratio (K_2O/Na_2O = 1.87 wt%). Trace element analysis reveals enrichment in incompatible trace elements for instance 372.60 ppm Rb, 37.69 ppm Th, and 422.90 ppm Zr with significant LREE enrichment relative to the HREE (La/Yb = 26.11). Depletion in Nb and Ta indicate an subduction related origin (Fig. 5).

4.2.2.2. Group 2B trachytic tephras with low alkali ratio. The high-K trachytic glass shards of Group 2B (61.96–62.93 wt% SiO_2; 6.19–6.59 wt% K_2O) contain higher Na_2O (7.27–8.05 wt%) than K_2O content, resulting in a distinctly low alkali ratio (K_2O/Na_2O = 0.81–0.85 wt%). These Group 2B shards are found in cryptotephra layers in Lake Lia between 612 and 613 cm depth (LIA_613 and 612).

4.2.3. Uncorrelated glass shards (UCG) with mixed geochemistry

This group is composed of both rhyolitic and trachytic glass shards at the several stratigraphically different depths in both Lake Lia and Brazi. The various differences in geochemistry that do not fit into the previously described groups. A single rhyolitic shard from Lake Lia at 607 cm depth (LIA_607) exhibits lower SiO_2 (73.05 wt%), high K_2O (5.22 wt%), high FeO_t (3.62 wt%; Fig. 4A and B) compared to potential group

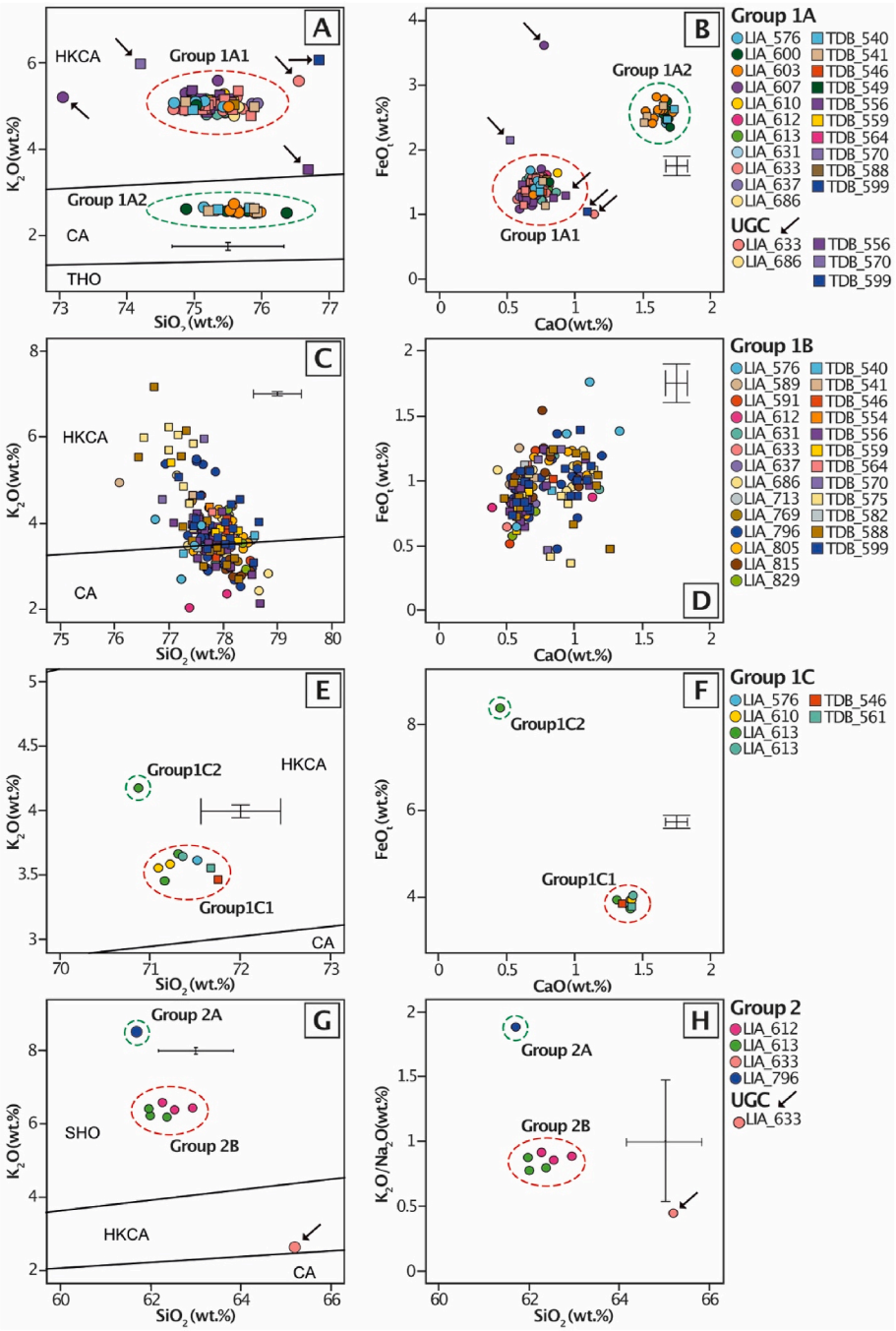

Fig. 4. Major element bi-plots of individual glass shards arranged by geochemical compositional groups from cryptotephra layers of Lakes Lia and Brazi. Arrows in figure A, B, G and H highlight individual analysis related to Group 3. THO = tholeite series, CA = calc-alkaline series, HCKA = high-K calc-alkaline series, SHO = Shoshonite series. SiO_2 versus K_2O series classifications follow Peccerillo and Taylor (1976).

equivalents of Group 1B. LIA_633 also contains a single rhyolitic shard with higher SiO_2 (76.55 wt%), high K_2O (5.60 wt%), and low FeOt and CaO (1.00 wt% and 1.14 wt% respectively). In addition, a single analysis from LIA_686 with similar SiO_2 (74.62 wt%), yet lower K_2O (4.62 wt%) content, displaying an HKCA affinity was also identified (Fig. 4A and B). A single trachytic shard from LIA_633 is also assigned to this group, with higher SiO_2 (65.17 wt%), with lower Na_2O (5.95 wt%), and lower K_2O (2.64 wt%) producing a very low alkali ratio of 0.44 wt% (K_2O/Na_2O), making it a distinctly different population from Groups 2A and 2B.

In Lake Brazi, a distinct single rhyolitic (SiO_2 74.20 wt%) glass shard from TDB_570 displayed particularly high K_2O (6.00 wt%) and FeO_t (2.15 wt%) content and resides on the HKCA/shoshonitic boundary (Fig. 4A and B). While a single rhyolitic shard in TDB_599 (SiO_2 76.85 wt %) exhibits similar K_2O (6.09 wt%) content but lower FeO_t (1.04 wt%) content.

5. Interpretation and discussion

5.1. Identifying primary and secondary cryptotephra deposits

In an ideal cryptotephra concentration profile, the largest peak in shard concentration can be described as an isochron, in addition to peaks preceding the sterile sediment. This implies primary tephra deposition, and therefore can be directly associated with the timing of a

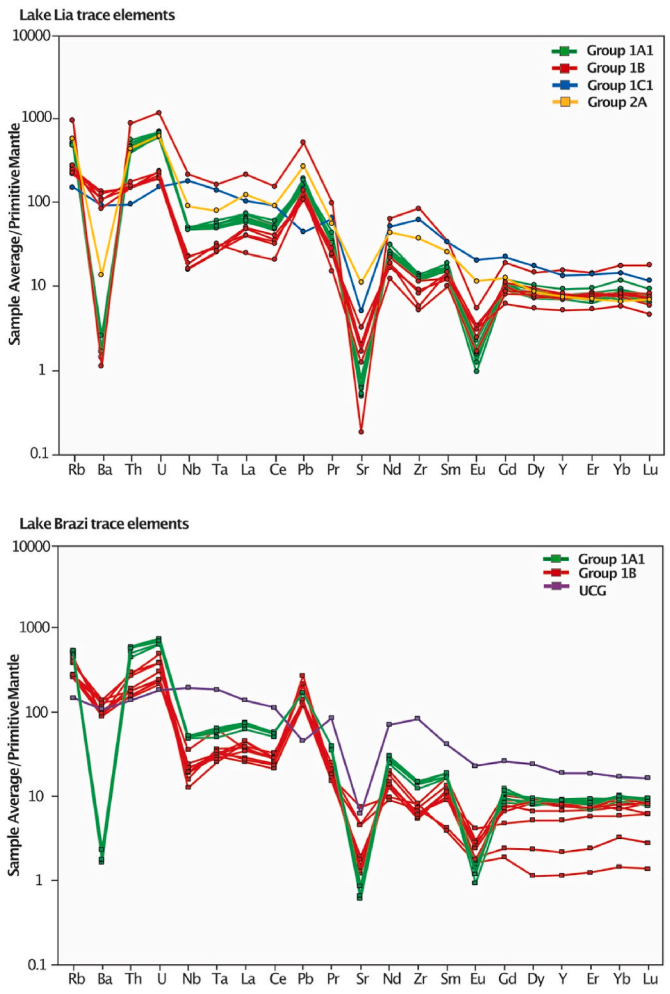

Fig. 5. Trace element mantle-normalised (Sun and McDonough, 1989) profiles of cryptotephra deposits identified and extracted from both Lakes Lia and Brazi. Glasses are assigned to their respective groups.

volcanic eruption itself (Lowe, 2011; Davies et al., 2012). In reality, within lake sediment records, lower shard concentrations are often seen to underlie and overly distinct peaks and may be associated with taphonomic processes such as bioturbation and redistribution of sediment by underwater currents (Pyne-O'Donnell et al., 2008; Davies et al., 2012). Secondary mobilisation of shards from the surrounding local catchment due to erosional events and melting snow-beds and/or melting lake ice cover can also result in the input of glass shards up a profile (Hunt, 1994; Bergman et al., 2004; Davies et al., 2007; Harning et al., 2018). Coring-related reworking is largely excluded due to the sampling procedure undertaken of taking sediment from the central part of the core, avoiding contamination.

There are two very clear shard peaks identified from the shard concentration profiles of Lakes Lia and Brazi with at depths of 603 cm (LIA_603) and 564 cm (TDB_564), respectively (Fig. 2). The largely homogenous geochemistry and similar shard morphologies allow these depths to be interpreted as robust isochrons. Additional primary isochrons can be seen in Lake Lia where sterile sediment precedes the peak and is largely dominated by a homogenous geochemistry (e.g. LIA_637). In both lake profiles, where there are near identical peak shard concentrations at adjacent 1 cm resolution sample depths, exhibiting largely homogenous geochemistry, the position of the isochron is taken as the mid-point of these depths. This is seen with TDB_541 and TDB_540 (i.e. 'TDB_540.5') while in Lia, samples LIA_613 and LIA_612 yield an isochron defined as 'LIA_612.5' (with a sterile shard profile immediately below these depths (Fig. 2).

However, the constant low shard concentration profiles and associated low peaks of Lia and Brazi likely show reworked tephra. Lake Brazi especially shows continuous (background) tephra deposition throughout the sediment record. The mixed geochemistry and shard morphologies seen in many of the depth intervals analysed highlights the potential of secondary re-mobilisation of glass shards (e.g. LIA_805, LIA_796, LIA_589, TDB_588, TDB_556, TDB_546). In both lake records, glass shards chemically consistent with the clearly defined isochrons, such as LIA_637 and TDB_564, are interpreted as the pro-longed in-wash of shards from the surrounding lakes' catchments, probably due to melting snow beds or ice.

Davies et al. (2007) have highlighted that the presence of snow-beds can become 'tephra traps' and, with subsequent melting, release tephra into the catchment and lake over an extended period after the primary deposition. Multi-proxy evidence from Lia and Brazi indicates the presence of prolonged snow-beds within the catchments, particularly during the early part of the Younger Dryas period which saw an increase in melting around the time of the primary isochron deposition of LIA_637 and TDB_564 (Buczkó et al., 2009; Magyari et al., 2009, 2012; Finsinger et al., 2018). In addition, there was a rock glacier located on the western side of Lake Lia during the Last Glacial period (Urdea, 2004). A glacier is also located near Lake Bucura, which would have influenced inflow to Lia (Urdea, 2004). These glaciers could also be interpreted as 'traps' for tephra shards, which would then be released into the catchment with melting and subsequently deposited into the record (Davies et al., 2007). This is hypothesised due to the continuous lower shard concentrations of heterogeneous glass chemistry within both lake profiles, making identification of clear isochrons difficult.

5.2. Chronological modelling

The output from the new comprehensive Bayesian age model for Lake Lia and Lake Brazi incorporates the cross correlation of the previously identified isochron of the Askja-S from both sites (Kearney et al., 2018) to improve their age-depth models (Fig. 6). The age derived for the Askja-S tephra in this study is given as 11,070–10,720 cal BP (Table 3). This is in good agreement with the previous, higher precision estimate produced by Kearney et al. (2018) of 10,824 ± 97 cal BP (2σ) that utilises data from additional sites, but models on to IntCal13, although the two calibration curves are essentially identical at this point in time.

The subsequent newly discovered tephra layers identified as representing primary deposition, and therefore isochrons, can be dated from both sites (see Table 3 and section 5.3). Comparing the output ages from both sites, Lia has larger age uncertainties compared to Brazi, particularly for the Late Glacial tephra layers of Lia (Table 3 and Fig. 6). This can be attributed to the lack of radiocarbon dates located close to the depths of where these tephras were found (Fig. 6). Hubay et al. (2018) highlighted the lack of organic material at this time to provide reliable radiocarbon dates. This is in contrast to Brazi with several macrofossils' radiocarbon dated throughout the record (Fig. 6, Hubay et al., 2018). We therefore suggest that the ages produced by Brazi are more reliable for dating the Late Glacial tephra layers reported in this study. However, during the Early Holocene period of Lia, additional reliable radiocarbon dates improve the chronological uncertainty for tephra layers identified in this part of the core. There is potential to improve the Late Glacial part of Lia's age-depth model by correlating the identified tephra layers reported here to another well-dated record in future.

5.3. Cryptotephra correlations

5.3.1. Group 1A1 (Lipari, Aeolian Islands, Italy)

The rhyolitic shards with high K_2O content (HKCA) of Group 1A1 correlate well to the HKCA rhyolites from Lipari, Aeolian Islands (Fig. 7A and B; Albert et al., 2012; McGuire et al., 2022). These shards

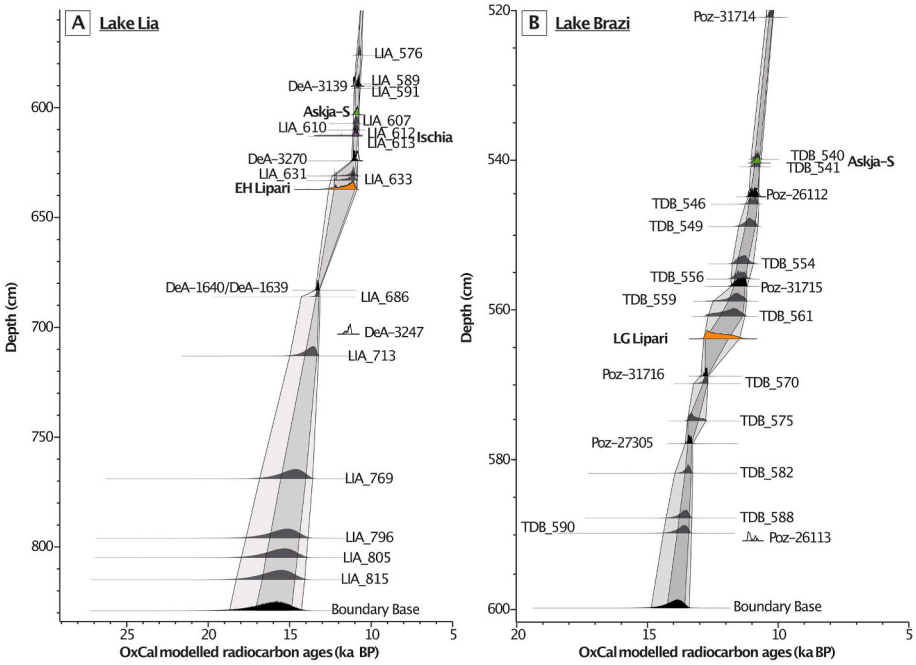

Fig. 6. Bayesian chronological model output for (A) Lake Lia and (B) Lake Brazi using radiocarbon dates (Hubay et al., 2018) and the previously identified isochron of Askja-S (Kearney et al., 2018) modelled on the updated calibration curve, IntCal20 (Reimer et al., 2020). Isochrons of the LG Lipari and Ischia-sourced tephras are highlighted in colour with visual display of the ages for the remaining tephra peaks geochemically identified in both records. Dark grey and light grey show 68.2% and 95.4% highest probability density ranges, respectively. Unmodelled radiocarbon ages are highlighted with as black and white (as seen with outlier DeA-3247).

are found across several depths in the LGIT studied sediments of Lakes Lia and Brazi (Fig. 2).

A clear isochron of Lipari-type Group 1A1 shards is identified in Brazi at 564 cm depth (TDB_564) during the Younger Dryas period (Fig. 2), and is dated by pollen stratigraphy and radiocarbon dating to between 12,885–11,515 cal BP (Fig. 2, Table 3; Magyari et al., 2009). In Lake Lia, at 637 cm (LIA_637) a Lipari-type isochron is identified, whilst the peak is not as pronounced as the layer in Lake Brazi, this Lipari-type deposit in Lake Lia is preceded by sediments completely sterile of glass sahrds (Fig. 2). Shards with similar Lipari-type compositions extending across a broader sediment interval above this initial depth (LIA_637), including analysed intervals of 633 cm (LIA_633) and 631 cm (LIA_631; Fig. 2).

In contrast to Lake Brazi, in Lake Lia this Lipari-type layer at 637 cm is chrono-stratigraphically positioned at the Early Holocene transition according to the pollen-stratigraphy and has a modelled age of 12,590–10,845 cal BP (Fig. 2; Table 3). Despite overlapping age uncertainties, this pollen-stratigraphy offset between the Lipari-type isochrones in Lake Brazi (564 cm) and Lia (637 cm) potentially indicates ash fall from two separate Lipari eruptions recorded in the region.

In both Lia and Brazi, glass shards of Lipari geochemistry are seen throughout depths after these isochrons. This may hamper finding the LIA_637 equivalent in age in the Brazi record against a background of constant shard inwash (see section 5.1). The lack of the older LG TDB_564 Lipari tephra equivalent in Lia could be due to Lia being covered by glacier/ice at the time of eruption in the Younger Dryas due to being at higher elevation and so was not deposited within the sediments (Magyari et al., 2009, 2012).

HKCA explosive rhyolitic eruptions on Lipari have occurred periodically through approximately the last 40 kyr (Forni et al., 2013; Albert et al., 2017). The distal occurrences of these tephras are mainly limited to marine records in the Tyrrhenian, Adriatic and Ionian Seas (e.g. Paterne et al., 1988; Siani et al., 2004; Caron et al., 2012; Albert et al., 2017) with only limited occurences in distal terrestrial records (e.g. Narcisi, 2002; Di Roberto et al., 2018). The most widely traced rhyolitic tephra sourced from Lipari relates to the early Holocene 'Vallone del Gabellotto' (VdG) eruption dated at 8,430–8,730 cal BP (Siani et al., 2004; Albert et al., 2017). However, more recently distal sediment records hae revealed evidence for other widespread rhyolitic ash fall events from Lipari, chronologically older than the VdG tephra.

Indeed, a LGIT aged Lipari cryptotephra layer has been identified by Albert et al. (2017) stratigraphically below the VdG within the sediments of an Ionian Sea marine core M25/4–12 (44 cm), this tephra was chrono-stratigraphically positioned using the core's oxygen isotope stratigraphy (Negri et al., 1999). Trace element results show a subtly lower LREE concentrations compared to VdG (Fig. 6D-E; Albert et al., 2017).

In addition, two LGIT age Lipari tephra layers have also been identified by trace element analysis at Lake Ioannina, Greece, these are indistinguishable in major elements compositions from the overlying VdG tephra also recorded at the site (McGuire et al., 2022). Correlating Lia and Brazi Lipari tephras to a precise Ioannina Lipari layer is difficult, even with using trace element compositions due to the overlap in the glass chemistries of both pre-VdG distal tephra, IO8T_16.07 and IO8T_15.23 at Ioannina (McGuire et al., 2022; Fig. 6D and E). The Ioannina record also provides imprecise age estimates for these two proposed Lipari eruptions (12,470–10,210 cal BP and 10,650–8,520 cal BP, respectively) both of which broadly overlap with the ages of TDB_564 and LIA_637. Unfortunately, the chronology of the Ioannina sequence is poorly constrained during the LGIT period, with radiocarbon dates being affected by a 'hard water' effect (Lawson et al., 2004; McGuire et al., 2022). In combination with the similar compositional data, this makes a robust correlation to either IO8T_15.23 or IO8T_16.07 difficult, indicating that further investigation is needed. Nonetheless, it is tentatively proposed that TDB_564 (termed LG Lipari) tentatively correlates to the older Lipari layer of Ioannina IO8T_16.07 and M25/4-12-44 cm with LIA_637 to IO8T_15.23.

Chrono-stratigraphically below the Lipari isochrons resolved in Lake Brazi (TDB_564) and Lia (Lia_637) respectively, are small peaks containing minor HKCA rhyolitic glass shards components mixed with other glass chemistries. These were observed in Lake Lia at LIA_686 and Brazi TDB_588 (Figs. 2, Fig. 7A-B, Hubay et al., 2018). Only two HKCA shards

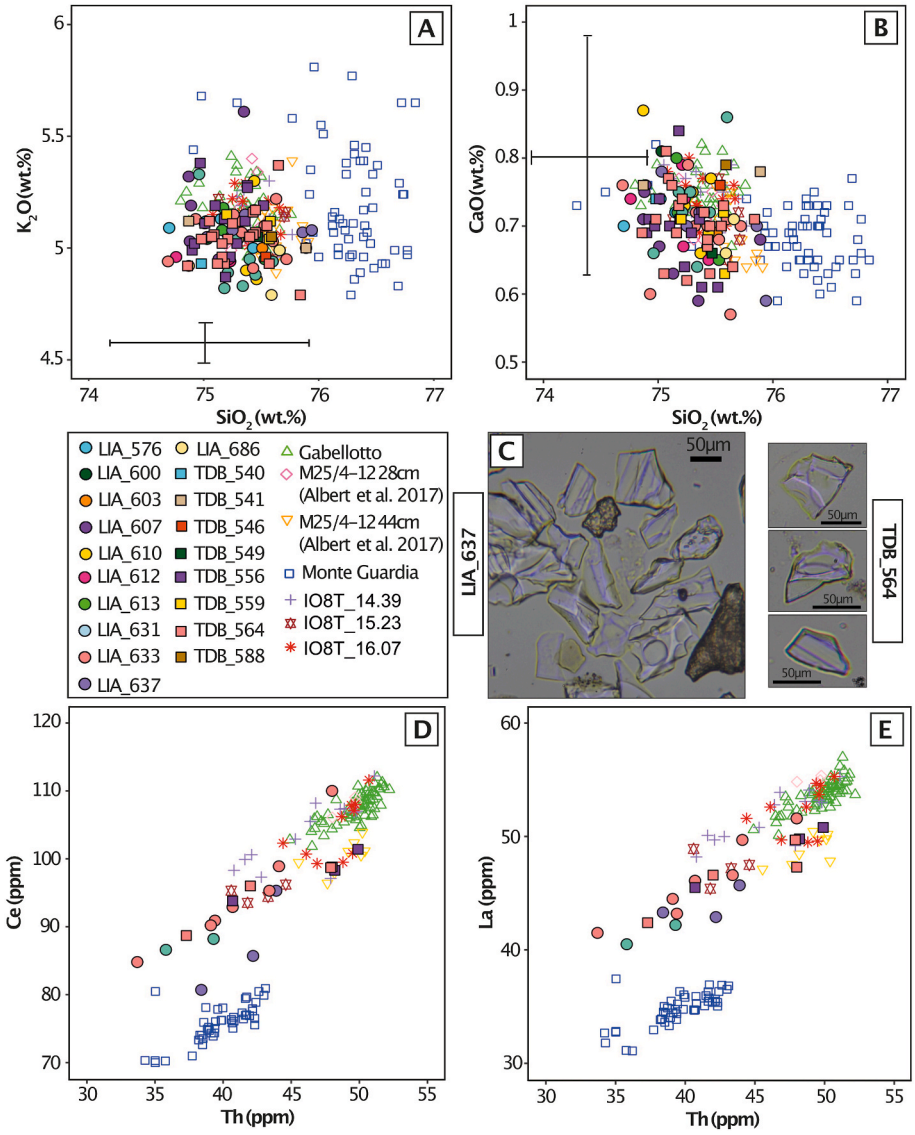

Fig. 7. Major element biplots showing the main geochemical characteristics of Group 1A1 shards from both Lia and Brazi (A–B) with trace element date from selected depths (D–E) and subsequently correlated to known eruptions from Lipari, Aeolian Islands from the last 30 ka (Albert et al., 2017). Additional trace element evidence for a LG Lipari eruption is from Ioannina (McGuire et al., 2022). Photos of LG Lipari glass shards are also presented from both cores (C). Error bars represent 2 standard deviations of repeat analyses of the MPI-DING StHs6/80-G glass standard on the major element graphs. Error bars on the trace element graphs were smaller than the symbols and are not presented.

are found in LIA_686 with one in TDB_588 mixed amongst other glass chemistries. These shards did not undergo trace element analysis.

In Lia, there sterile glass-free sediments between the LG Lipari isochron (LIA_637) and the older LIA_686 depth, combined with their positions in different climato-stratigraphic zone (pollen) suggest the possibility of earlier Lipari eruptions recorded in the region. However, in these deeper intervals, the Lipari-type glasses are subsidiary components, reflected by the very minor number of analyses, as such it is difficult to use these horizons to provide clear evidence of additional older eruptions on Lipari recorded in the region. Given the very low Lipari glass shard numbers, we cannot rule out that core-related displacement has resulted in these stratigraphically older Lipari-type composition shards from the LGIT Lipari peaks of LIA_637 and TDB_564. The absence of tephra in laboratory blanks reduce the likelihood of contamination.

Nevertheless, we can propose, using stratigraphic and chronological evidence from both Lake Lia and Brazi, that there are at least two Lipari eruptions responsible for widely dispersing ash during the LGIT: 1) the Younger Dryas TDB_564 (12,885–11,515 cal BP) isochron seen in Brazi and; 2) The Late Glacial/Early Holocene transition isochron of LIA_637 (12,590–10,845 cal BP). At source, there is an absence of a prominent or widely trace eruption unit on the island in correct chrono-stratigraphic position between the 'Monte Guardia' eruption (ca. 27 ka BP) and the VdG. The patchiness of near-source volcanic stratigraphies is not uncommon, particularly on volcanic islands, owing to limited on-land exposures, with much of the erupted material possibly entering the sea (Albert et al., 2012; Cassidy et al., 2014). This highlights the importance of distal sedimentary records for understanding past eruption frequencies of volcanic centres. The rhyolitic HKCA Lipari-derived TDB_564 cryptotephra clearly presents a useful tephrochronological marker for the Mediterranean region capable of synchronising sedimentary archives in the LGIT period.

5.3.2. Group 1A2 rhyolites (Askja-S, Askja, Iceland)

Previous identification of LIA_603 and TDB_540.5 as distinct isochrons correlated to the Askja-S tephra has been made by Kearney et al.

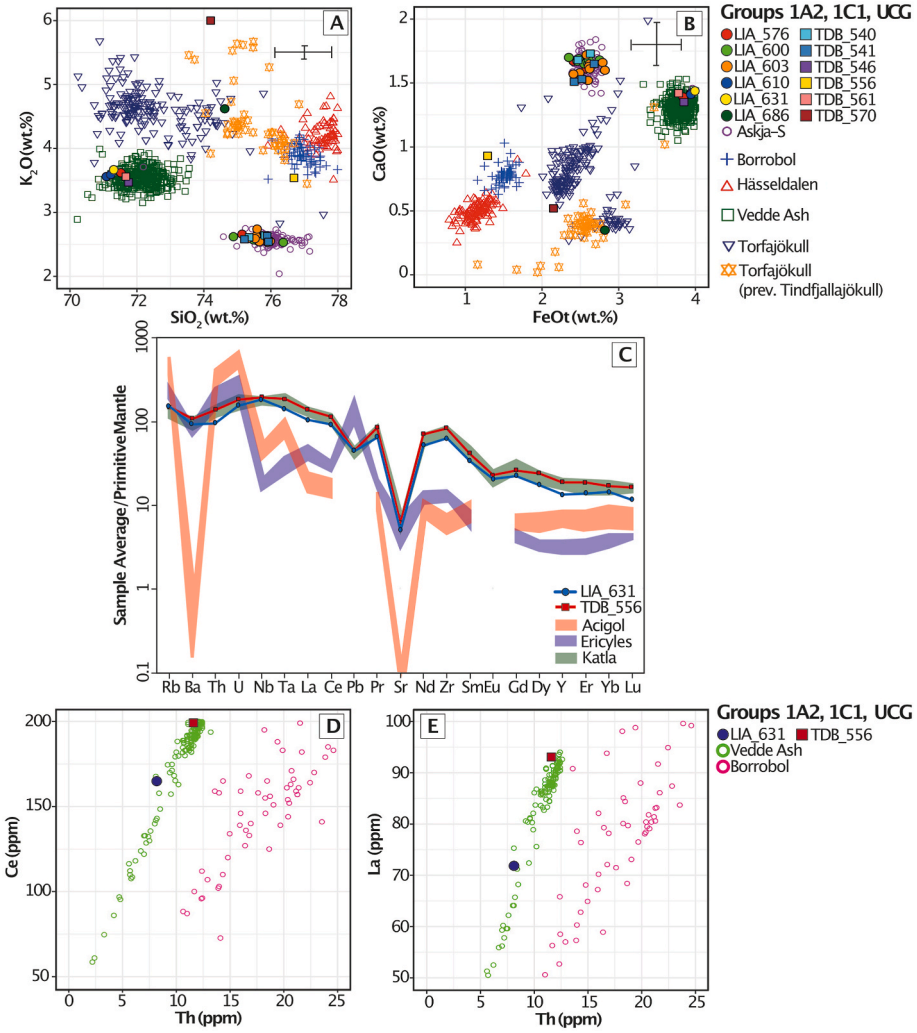

Fig. 8. Geochemical bi-plots of (A–B) the major elemental data from Lakes Lia and Brazi shown alongside geochemically grouped shards associated with known LGIT rhyolitic eruptions from Icelandic volcanoes: Borrobol (Turney et al., 1997; Davies et al., 2003; Matthews et al., 2011; Pyne-O'donnell, 2011; Lind et al., 2016); Vedde Ash (Birks et al., 1996; Davies et al., 2005; Blockley et al., 2007; Lane et al., 2011; Lane et al., 2012a, 2012b; Wastegård, 1998; Wastegård et al., 2000, 2000, 2000); Torfajokull/Tindfjallajokull (Moles et al., 2019; Ram et al., 1996); Hasseldalen (Davies et al., 2003; Lind and Wastegård, 2011; Housley et al., 2013; Lane et al., 2012a; Lilja et al., 2013; Larsen and Noe-Nygaard, 2014; Wulf et al., 2016a); Askja-S (Davies et al., 2003; Sigvaldason, 2002; Turney et al., 2006; Lane et al., 2011a; Lind and Wastegård, 2011; Wulf et al., 2016a; Jones et al., 2017; Kelly et al., 2017; Lowe et al., 2017). Error bars represent 2 standard deviations of repeat analyses of the MPI-DING StHs6/80-G glass standard on the major element graphs. C) Trace element profiles of LIA_631 and TDB_556 glasses that underwent trace element analysis normalised to primitive mantle compositions (Sun and McDonough, 1989) with (D–E) compared to reference data from Tomlinson et al. (2015) from volcanoes that produce high silica glasses.

(2018). Further Askja-S type shards are seen higher up the stratigraphy in Lia only at LIA_600 and LIA_576 (Figs. 2 and 8) and labelled as compositional group 1A2. Whilst other, younger tephra deposits from Askja volcano have been reported in the Holocene (e.g. the Askja-L and Askja-H; (Jóhannsdóttir, 2007; Striberger et al., 2012; Gudmundsdóttir et al., 2016), there is no evidence to date of these tephra deposits having been identified beyond Iceland. This strongly suggests that these shards are possibly reworked from the earlier, primary airfall deposit of the Askja-S tephra in the catchment of lake Lia. No further samples were geochemical analysed above TDB_541 in Brazi in this study.

5.3.3. *Group 1B (Anatolian unknown eruption(s), Turkey)*

The high SiO_2 composition of Group 1B represents highly evolved rhyolitic volcanic glass. Within these glass populations there is a variation in K_2O content, ranging across the CA/HKCA boundary. This divergence in K_2O may reflect late-stage fractionation (K-feldspar) or distinctly different magmas from different but chemically similar volcanic sources.

Several volcanoes are known to have produced high-silica rhyolites (>76 wt%) during the Late Glacial period. Volcanic sources from the Aeolian Islands, including Lipari, Vulcano and the Salina Islands, are known to have erupted evolved rhyolitic magmas in the last ~15kyr (Albert et al., 2015, 2017). However, tephra deposits produced by Lipari and Vulcano exhibit lower SiO_2 (75–76 wt%) and higher FeO_t (>1.5 wt %) content than Group 1B glasses. Salina has also produced variable high SiO_2 (70–77 wt%) with higher CaO (~1.3 wt%) than the Brazi and Lia Group 1B glasses described (Albert et al., 2017). The Aegean Arc volcanoes of Nisyros and Kos have also produced similar high SiO_2 content tephra yet have higher CaO (>1.1 wt%) and lower FeO_t (<0.75 wt%) (Fig. 9; Tomlinson et al., 2012a; Karkanas et al., 2015; Satow et al., 2015).

Far travelled ash from Icelandic volcanic eruptions during the LGIT has been recorded as far south as the Italian Alps (e.g. Lane et al., 2012b, c) and at Lakes Lia and Brazi (the Askja-S tephra, as previously reported by Kearney et al. (2018)). The Icelandic Borrobol and Hässeldalen cryptotephra deposits found across Europe from unknown specific volcanic

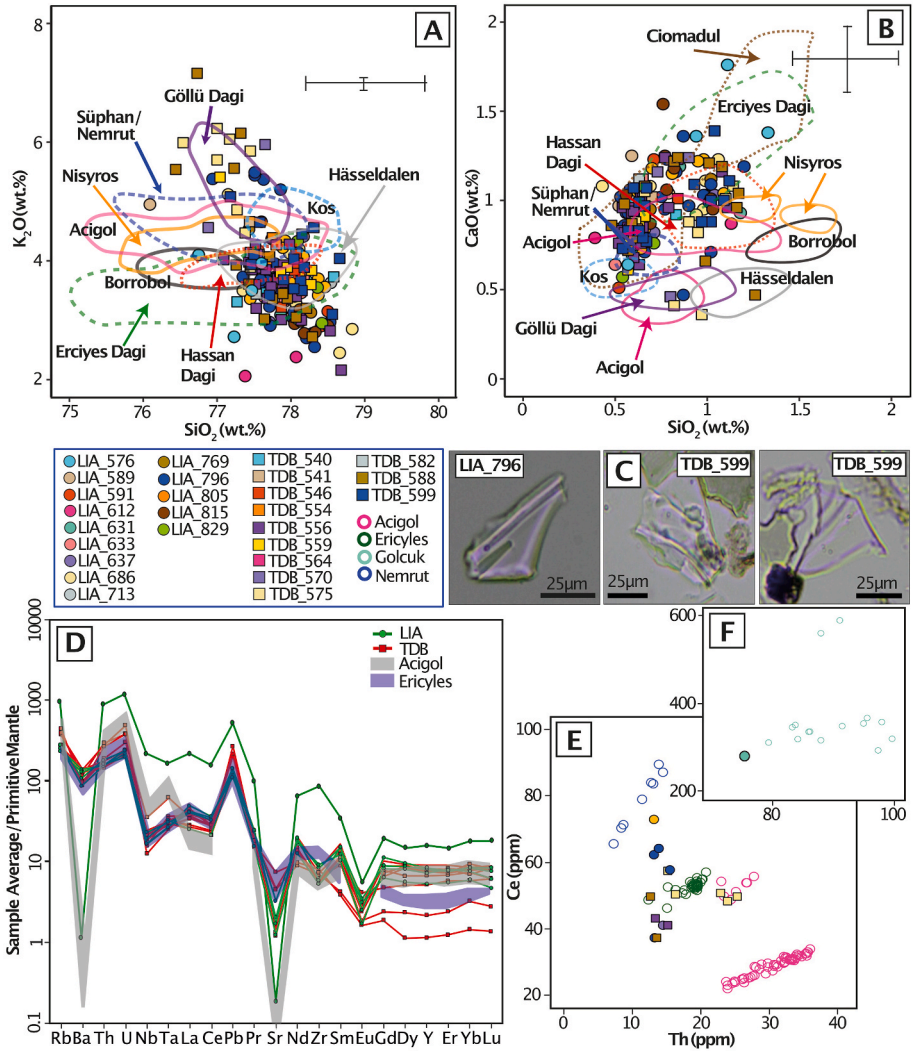

Fig. 9. A–B) Major element bi-plots of high silica glass shards from Lakes Lia and Brazi compared to similar high silica glass shards from: Ciomadul, Romania (Karátson et al., 2016); Anatolian tephras from Acigol, Erciyes Dagi, Hassan Dagi and Gollu Dagi (Tryon et al., 2009; Hamann et al., 2010; Cullen et al., 2014; Barton et al., 2015; Tomlinson et al., 2015; Neugebauer et al., 2017, 2021); Icelandic tephra units of Hasseldalen and Borrobol (no exact Icelandic volcanic source; Turney et al., 1997; Davies et al., 2003; Pyne-O'Donnell, 2007; Lind and Wastegård, 2011; Matthews et al., 2011; Lane et al., 2012a; Housley et al., 2013; Lilja et al., 2013; Lind et al., 2016; Wulf et al., 2016a; Cook et al., 2018); Aegean Arc tephras from Nisyros and Kos (Eastwood et al., 1999; Kwiecien et al., 2008; Tomlinson et al., 2012a; Karkanas et al., 2015; Satow et al., 2015). Error bars represent 2 standard deviations of repeat analyses of the MPI-DING StHs6/80-G glass standard. C) Photographs of these glass shards from certain depths in Lia and Brazi. D, E, F) Trace element profiles of Lake Lia and Brazi glasses that underwent trace element analysis normalised to primitive mantle compositions (Sun and McDonough, 1989) with comparisons to reference data from Tomlinson et al. (2015) from volcanoes that produce high silica glasses.

sources are similar in geochemistry to Group 1B (Lind et al., 2016; Cook et al., 2018; Wastegård et al., 2018). These tephras have similar high-silica compositions (>76 wt%), but can be discriminated easily from Group 1B by comparing FeO_t and CaO content, indicating that known Icelandic volcanoes are not the source for these cryptotephra deposits.

Further evidence of a different volcanic source for Group 1B high-silica glasses is provided by trace element composition. Trace element analysis was conducted on multiple volcanic glasses at depths associated with Group 1B high-silica rhyolites from both lakes. Results indicate a continental subduction setting with a depletion in Nb and Ta, and with an enrichment of Th (Fig. 9; Tomlinson et al., 2015). This further confirms that Icelandic volcanoes are not the source for these glass shards.

The nearest volcano with a continental subduction setting is Ciomadul, Romania. The chemical compositions of Ciomadul glass shards to Group 1B are similar but have a subtle offset (Fig. 9A and B). The timing of known volcanism at Ciomadul precludes Lake Lia and Brazi correlations, with the most recent explosive eruption dated to 31.5–27.7 ka BP (Karátson et al., 2016; Wulf et al., 2016b; Harangi et al., 2020).

With the exclusion of Carpathian subduction-related rhyolites, Italian and Aegean Arc settings, the next plausible source region for subduction zone volcanoes is Anatolia. Glass shards with HKCA affinity are similar in composition to tephra deposits from Acigöl, Ericyles Dagi and Göllü Dagi in the Central Anatolian Volcanic Province (Bakke et al., 2009; Hamann et al., 2010; Zanchetta et al., 2011; Tomlinson et al., 2015). Nemrut, located in the Eastern Anatolian Volcanic Province (EAVP), has produced tephras with less evolved compositions (<76 wt %; Cullen et al., 2014; Schmincke and Sumita, 2014). Other volcanoes located in the EAVP and Western Anatolian Volcanic Province currently lack sufficient published glass chemistry data to allow a comparison to Group 1B, particularly glass shards with a CA affinity (Pearce et al., 1990; Yılmaz et al., 1998; Cullen et al., 2014; Schmincke and Sumita, 2014; Neugebauer et al., 2021).

Identifying a precise geochemical correlation of Group 1B glasses to a volcano and/or eruption from the Anatolian region is extremely challenging. Firstly, this region lacks proximal volcanic glass geochemistry (major, minor and trace elements). This is exacerbated by

limited stratigraphic and geochronological constraints on past volcanic activity (proximal and distal) (Cullen et al., 2014; Neugebauer et al., 2021). In addition, there are multiple shard peaks of mixed >76 wt% SiO_2 chemistry within the lower depths of both Lakes Lia and Brazi. It is unclear if this is due to constant secondary inwash from snow-traps or production of geochemically similar tephra from a volcano or volcanoes. Previous research has highlighted that many volcanic systems can produce similar major and minor element glass chemistries over prolonged timescales (e.g. Smith et al., 2011; Lane et al., 2012b; Karátson et al., 2016; Cook et al., 2018). Trace element analysis can help distinguish between eruptions (Tomlinson et al., 2015; Albert et al., 2015), although certain volcanoes can also produce identical trace element compositions with each eruption (e.g. Lane et al., 2012c; Cook et al., 2018) resulting in unclear correlations to specific eruptions. This could be the case for the Anatolian region. However, current trace element analysis from this study and comparison to limited published data, show at least three shards in TDB_575 having a strong geochemical correlation to Acigöl, Central Anatolian Volcanic Province (Fig. 9D–F). In addition, a single shard from LIA_631 suggests an origin from Western Anatolian Volcanic Province as indicated by trace element results (Fig. 9D–F). Yet, once again, a direct attribution to an eruption cannot be made at this time due to the lack of currently glass geochemistry from volcanoes in this region.

Nonetheless, the geochemical evidence presented from Lake Lia's and Lake Brazi's high-silica rhyolites suggests, via the process of source elimination of Italian, Icelandic and Aegean volcanic sources, that Central Anatolian volcanoes are the most likely ash sources. That is despite being ~1,000 km away.

5.3.4. Group 1C1 (Katla-type, Katla, Iceland)

The glass shards of Group 1C1 exhibit glass a chemistry similar to the rhyolitic products of Katla volcano, Iceland (e.g. Vedde Ash, Dimna Ash; Fig. 8A and B). Trace element analysis conducted on a single Katla-type shard in LIA_631 provides further evidence for the correlation to this volcano (Fig. 8C–E).

The chrono-stratigraphic position of these Group 1C1 shards in both Lia and Brazi suggest a Younger Dryas (GS-1) to Early Holocene transition deposition (Fig. 2). During the LGIT period, multiple tephra units were produced by Katla volcano displaying similar rhyolitic chemical compositions recorded at sites across Europe (e.g. Bond et al., 2001; Pilcher et al., 2005; Thornalley et al., 2011; Matthews et al., 2011; MacLeod et al., 2015). This includes the Vedde Ash, which is traced across northern (e.g. Birks et al., 1996; Timms et al., 2018), central (e.g. Blockley et al., 2007; Lane et al., 2013) and southern European regions (e.g. Lane et al., 2012a; Lane et al., 2012c) with extension into western Russia (e.g. Wastegård et al., 2008, 2000; Haflidason et al., 2019). Recentlly, the Vedde Ash has been identified in Lake Latoritei, Romania (Szabó et al., 2023). The Vedde Ash has been radiocarbon dated to 12,100–11,915 cal BP (95.4% range; Bronk Ramsey et al., 2015) and has an age of 12,171 ± 114 b2k (maximum counting error, MCE equivalent to 2σ) in the Greenland ice cores, where it occurs in the middle of GS-1 (GICC05, Rasmussen et al., 2006). Two deposits with Katla-type shards in Lake Lia and Brazi overlap in age estimates with the age for the Vedde Ash, LIA_631 and TDB_561 (see Table 3). However, only TDB_561 is stratigraphically positioned in the Younger Dryas period while LIA_631 is within the Early Holocene period (Fig. 2). The single shard of TDB_561 is most likely correlated to the widespread Vedde Ash. However, with only one shard being identified, no isochron is drawn from this depth.

The age estimates of LIA_631, LIA_613, LIA_610, LIA_576 and TDB_546 produced in age models from the present study (Table 3, see section 5.3), along with locally described pollen zones (Magyari et al., 2009, 2012; Vincze et al., 2017), show that these cryptotephra deposits are too young to represent primary deposition of the widespread Vedde Ash. While younger Katla-type tephra have been identified post the Vedde Ash in many cryptotephra records in northern Europe. For example the younger Abernethy Tephra, dated to 11,584–11,340 cal BP (Bronk Ramsey et al., 2015) are restricted to sites in north-west Europe (Matthews et al., 2011; MacLeod et al., 2015; Timms et al., 2018; Jones et al., 2018), making it unlikely that the younger Katla-type deposits in Lake Lia and Brazi are from potential smaller magnitude eruption of Katla during this younger time frame. Several authors have identified single Katla-type shards within European records as well during the Early Holocene (e.g. Timms et al., 2017, 2018; Jones et al., 2018). However, re-working of underlying Vedde Ash material has been suggested to be responsible for these isolated shards from these studies, rather than a primary deposit from the Abernethy Tephra eruption or an unknown Katla eruption.

The most likely explanation for these successive identifications of Katla-type glass chemistries in both the Lia and Brazi lake sequences is re-working and secondary deposition of Vedde Ash material from within the lake catchments, most likely from melting ice and/or snow beds (see section 5.1; Hunt, 1994; Bergman et al., 2004; Davies et al., 2007; Harning et al., 2018). Additional evidence that supports this interpretation includes: 1) very low shard concentrations of Katla-type glass geochemistry (1–2 shards) at different core depths in both lakes; 2) only the Vedde Ash having been traced into central-southern Europe (Blockley et al., 2007; Lane et al., 2012a, 2012b); 3) the inclusion of other mixed glass chemistries within the same cryptotephra layers examined and 4) the Vedde Ash has recently been identified in the region (Szabó et al., 2023).

As a result, the discovery of ash fall from the Katla eruption that produced the Vedde Ash indicates that it likely did reach further into the Carpathian Mountains, expanding evidence of this already extensive ash fall to southeastern Europe.

5.3.5. Group 1C2 (Unknown eruption, Pantelleria, Italy)

This single shard is an Fe-rich peralkaline rhyolite, identified as a pantellerite originating from Pantelleria Island, located in the Sicilian Channel (Fig. 10A–B, 10E). Volcanic activity has been recorded at this island throughout the Late Quaternary (MacDonald, 1974; Civetta et al., 1988; Tomlinson et al., 2015). The largest known caldera-forming eruption is the Green Tuff dated to 45,700 ± 500 ka by the $^{40}Ar/^{39}Ar$ technique (Scaillet et al., 2013). This tephra layer has been identified throughout the Mediterranean region (e.g. Paterne et al., 1988, 2008; Margari et al., 2007; Vogel et al., 2010; Tamburrino et al., 2012; Karkanas et al., 2015; Ntinou and Kyparissi-Apostolika, 2016).

Following this large-scale eruption, more localised pyroclastic and lava flows have been recorded during the LGIT period (Mahood and Hildreth, 1986; Civetta et al., 1988; Speranza et al., 2010; Neave et al., 2012). Previously, only one occurrence of distal ash from Pantelleria has been recorded. Magny et al. (2011) identified several pantellerite rhyolite shards in Lago Preola, southern Sicily, dated to 7,444–7,136 cal BP. This has been related to the VI cycle of volcanic activity from Pantelleria where K–Ar dating of lava flows places it in the LGIT period (Civetta et al., 1988; Neave et al., 2012). The single Pantellerite rhyolite shard from Lake Lia is significantly older at 11,120–10,745 cal BP. This chronologically coincides with the V cycle of volcanic activity of Pantelleria (Civetta et al., 1988). Dated lava flows do overlap in chronological uncertainty with the Lake Lia Pantellerite glass shard (Neave et al., 2012). However, no prominent explosive eruption deposits have yet been identified on the island, making a firm correlation challenging for now.

5.3.6. Group 2A (Campi Flegrei, Italy)

A single trachytic composition glass shard (LIA_796) is consistent with the product of Campi Flegrei caldera, Italy (Fig. 10A and B). The largest known eruption from the Campi Flegrei during the LGIT is that of the caldera-forming Neapolitan Yellow Tuff (NYT), this eruption has been dated to 14,433–13,795 cal BP (95.4%, IntCal13, (Bronk Ramsey et al., 2015) and is the most widely traced ash dispersal from Campi Flegrei during the LGIT (Lane et al., 2012a, 2015; Schmidt et al., 2002; Tomlinson et al., 2012b). While the single shard analysis of LIA_796 is consistent with the most evolved products of the NYT (Lower Member,

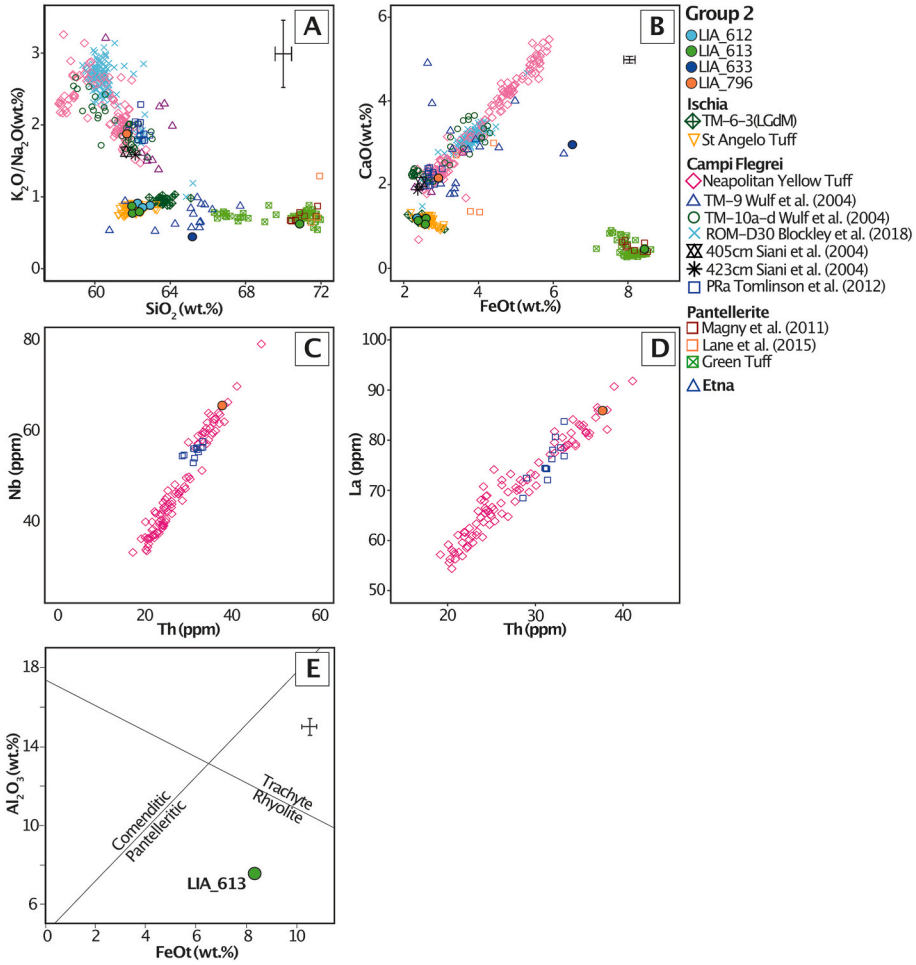

Fig. 10. (A-B) Major and trace element of glass shards from Lake Lia with comparisons to the Neapolitan Yellow Tuff from Campi Flegrei (Wulf et al., 2004; Magny et al., 2006; Lowe et al., 2007; Bourne et al., 2010; Lane et al., 2011b; Tomlinson et al., 2012a), known ash deposits pre-NYT (proximal deposit PRa, Tomlinson et al., 2012b; distal deposits TM-10a-d and TM-9 from LGdM Lago Grande di Monticchio (Wulf et al., 2004), 423 cm and 405 cm from MD909-17 (averages; Siani et al., 2004), and ROM-D30 (Blockley et al., 2018), known eruptions for Ischia (Wulf et al., 2008;TM-6-3 LGdM) and eruptions from Pantelleria (Margari et al., 2007; Vogel et al., 2010; Magny et al., 2011; Tamburrino et al., 2012) and Etna (Tomlinson et al., 2015). Error bars represent 2 standard deviations of repeat analyses of the MPI-DING StHs6/80-G glass standard. C-D) Trace element plots comparing LIA_796 to the Neapolitan Yellow Tuff (Wulf et al., 2004; Tomlinson et al., 2012b) and the limited glass chemistry available from PRa (Tomlinson et al., 2012b). Error bars were smaller than the symbols and are not presented. E) A single glass shard from Lake Lia cryptotephra peak LIA_613 plotted on the Peralkaline classification diagram following MacDonald (1974).

Fig. 10), a correlation to this eruption is problematic based on its climato-stratigraphic position in Lake Lia. LIA_796 is identified in the Older Dryas (Fig. 2), whereas the NYT is routinely identified in the sediments associated with the early Bölling-Alleröd (e.g. Siani et al., 2004; Schmidt et al., 2002; Lane et al., 2011b). A compositional similarity with the NYT is unsurprising as the evolved (trachytic) end-member of the NYT is not unique within the overall tephrostratigraphy of Campi Flegrei (e.g. Smith et al., 2011; Tomlinson et al., 2012b). Activity prior to the NYT at Campi Flegrei is characterised by a complex succession of eruption units, broadly termed the Tufi Biancastri (TB). This succession of eruption units extends between the NYT and Campanian Ignimbrite (Orsi et al., 1996). While the older portions of TB succession have been more recently characterised (glass chemistry; e.g. Tomlinson et al., 2012b), particularly in relation to the 29.3ka Masseria del Monte Tuff (Albert et al., 2019), the younger TB deposits remains poorly characterised at source. Consequently, we are only able to compare LIA_796 to a single chrono-stratigraphically relevant proximal TB eruption deposit from Ponti Rossi (PRa; Tomlinson et al., 2012b) which is dated at 16.1 ± 0.2 ka (Pappalardo et al., 1999). Widespread ash dispersals occurring shortly before the NYT, with a similar chemical signature (evolved end-member), are reported at LGdM (TM-9, TM-10a-d; Wulf et al., 2004), Grotta del Romito, Italy (ROM-D30; Blockley et al., 2018) and in two cores from the Adriatic Sea, MD909-17 (423 cm and 405 cm, Siani et al., 2004) and SA-03-11 (Matthews et al., 2015; Fig. 10).

Comparing of LIA_796 to the NYT/pre-NYT eruption deposits indicates a compositional similarity based on major and minor elements (Fig. 10A and B). Given LIA_796 comprises of only a single Campi Flegrei derived shard, and the limited amount of proximal glass data for the pre-NYT eruption units, a confident correlation is not possible (Fig. 10C and D). Furthermore, given only a single shard is identified, it is unclear if this can be confidently attributed to a primary ash fall deposit, and as such, it cannot be ascribed as an isochronous marker in Lake Lia's sedimentary record. Nonetheless, our finding provides further evidence for widespread ash dispersals associated with eruptive activity of Campi Flegrei in the period leading up to the NYT caldera-forming eruption during the LGIT (i.e. Siani et al., 2004).

5.3.7. Group 2B (Unknown eruption, Ischia, Italy)

Several K-rich trachytic glass shards were identified in two adjacent samples from Lake Lia (LIA_612 and LIA_613 – isochron position LIA_612.5), these trachytic glasses are consistent with those erupted in the Campanian volcanic zone. The high-Na content and subsequent low-alkali ratio (0.85 ± 0.10 wt%) preclude a link to Campi Flegrei, instead

the glasses are more consistent with eruptive products from Ischia Island (Fig. 10A-B; Paterne et al., 1988; Civetta et al., 1991; Wulf et al., 2008; Tomlinson et al., 2015). Ischia was active throughout the end of the Late Glacial and into the Holocene period (10 uncalibrated ^{14}C yrs BP -1302 AD; Civetta et al., 1991; de Vita et al., 2006). Within the annually laminated sediments of Lago Grande di Monticcio (LGdM) record (Wulf et al., 2008), three sub layers, TM-6-3, were attributed to unknown activity of Ischia and varve dated to 11,520 ± 580 cal BP (varves ± 5% error, Wulf et al., 2008). Additional shards displaying Ischia-like geochemistry are also found in Late Glacial sediments in the KET8004 Tyrrhenian Sea core (Paterne et al., 1988).

The modelled age for LIA_612.5 is 11,120–10,740 cal BP, with pollen and sediment stratigraphy confirming it as an very early Holocene tephra layer. This age overlaps in uncertainty with the age of TM-6-3 from LGdM (Wulf et al., 2008) and is certainly too young to relate to the older dated St. Angelo Tuff (15,820 ± 395 cal BP [varves, ±5% error], Wulf et al., 2008). To mitigate for potential Na_2O loss affecting the SiO_2 content (due to differing EPMA instrumental conditions, Hunt and Hill, 1996), geochemical comparisons between LIA_612.5 and TM-6-3 were made using CaO vs FeOt (Fig. 10). The apparent correlation in age and composition between LIA_612.5 and TM-6-3 provides further evidence for a major widespread ash dispersal originating from Ischia during the earliest Holocene period (Fig. 10).

5.3.8. Group 3 (Unknown eruptions, unknown volcanic sources)

There are several single rhyolitic glass shards at TDB_570 and LIA_686 that possess chemical compositions of possible Icelandic origin (Fig. 8A and B). However, correlating them to known Icelandic volcanic source(s) and/or eruption(s) is difficult. Yet, with the confirmed ultra-distal occurrence of the Askja-S tephra and Vedde Ash in both records, additional Icelandic eruptions may also be recorded at Lia and Brazi.

Tentative correlations of single glass shards from TDB_570 and LIA_686 can be made to the contentious Torfajokull volcano as a source for these shards (Fig. 8). The data for these correlations comes from the recently re-examined volcanic source for the Thórsmork Ignimbrite eruption by Moles et al. (2019) to Torfajokull rather than the previously attributed Tindfjallajokull volcano. Similar correlations were made to Torfajokull with rhyolitic shards of the Crudale Tephra from the British Isles by Timms et al. (2019). Both TDB_570 and LIA_686 plot within this volcano's chemical envelopes (Fig. 8). However, the modelled ages (13,270–12,720 cal BP TDB_570; 14,265–13,110 cal BP LIA_686) and Younger Dryas stratigraphy for both of these tephras is older than the proposed Crudale Tephra age, which is placed between 12,111 and 11,174 cal BP (Timms et al., 2019; Table 3). The Lia and Brazi tephras may present evidence for additional eruptions from Torfajokull during the LGIT. However, only single shards are present, and at different ages, in both sites. In addition, further geochemical and chronological examination of the Crudale Tephra and Torfajokull proximal outcrops needs to be undertaken before direct correlations to this volcano/eruption can be securely made.

The single glass shard from TDB_556 can be described as a "Borrobol-type" due to its correlation within the broad major and minor element geochemical envelopes of the distally-traced Borrobol-type tephra deposits found across NW Europe, for which no volcanic source is confirmed (e.g. Pyne-O'Donnell, 2007; Lind et al., 2016; Cook et al., 2018; Plunkett and Pilcher, 2018). There are distinctively lower FeOt and CaO compositions (Fig. 8A and B). Trace element data obtained from this shard further corroborates an Icelandic origin (Fig. 8C) however, comparisons to the Borrobol-type trace element data of Cook et al. (2018) sees no overlap in key elements, suggesting a different volcanic source, possibly Katla (Fig. 8C–E). In addition, the date for this Lake Brazi tephra is placed within the Early Holocene period and hence is significantly younger than the age of the Borrobol itself, which is dated within the LG (Bronk Ramsey et al., 2015). The volcanic source and eruption for this shard therefore TDB_556 remains unknown.

The additional single rhyolitic shards identified in TDB_599 and LIA_633, with the single trachytic glass shard from LIA_633, currently cannot be correlated to any known volcanic sources from the Anatolian, Italian, Aegean or Icelandic regions (Fig. 9). As a result, these tephra shards remain uncorrelated.

5.4. Expansion of the tephrostratigraphic framework

The records of Lake Lia and neighbouring Brazi have provided the first detailed LGIT tephrostratigraphy for Romania with four primary cryptotephra horizons successfully identified deriving from three different volcanic source regions: Askja, Iceland (TDB_540.5 and LIA_603); Lipari, the Aeolian Islands (Italy) (TDB_564 and LIA_637); and Ischia, the Campanian Volcanic Zone (Southern Italy) (LIA_612.5; Fig. 2). Additional potential important cryptotephra found includes the Vedde Ash, Iceland (TDB_561) and the NYT, Campanian Volcanic Zone (LIA_796). The Bayesian age-depth modelling performed, incorporating radiocarbon dating and cross-correlation of the Askja-S tephra from both sites, has provided refined ages for these eruptions. These important findings extend the European and Mediterranean tephrochronological framework eastward (Fig. 11).

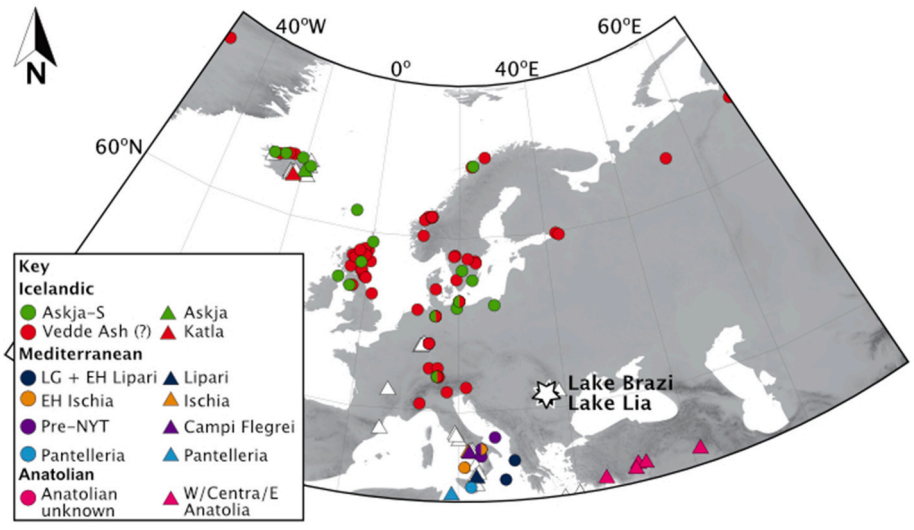

Fig. 11. Dispersal map of known LGIT tephras (individual circles) that have been found in Lakes Brazi and Lia. This includes volcanic ash dispersions from Iceland, Italy and Anatolia. Data from published resources.

Unfortunately, challenges still remain with the numerous glass shards identified in both Lake Lia and Brazi that exhibit various different geochemistries from unknown volcanic sources and/or eruptions. The continued use of the 15 μm sieve mesh size has shown to be crucial in retaining and subsequently identifying the finest grained ash particles produced (and transported) during some eruptions (<25 μm; Kearney et al., 2018), increasing the number of glass shards that could be geochemically analysed. Confidently correlating these glass shards to exact volcanoes/and or eruptions is limited due to the lack of proximal single glass shard geochemistry (major, minor and trace element data) for certain volcanic regions, most prominently Anatolia. The current lack of proximal glass geochemistry from these regions, coupled with a poor chronology of past eruptions from these volcanic sources, limits the potential of these tephras to provide regional markers and is a clear future endeavour to undertake. In addition, the taphonomic processes experienced at each site, particularly with regard to snow/ice trapping (section 5.1), are limiting because we cannot currently confidently identify the positioning of these isochrones currently within each record.

Yet, finding individual glass shards with compositions, confirmed with major, minor and trace element analysis, from Iceland, Italy and Anatolia do highlight the significant potential of the Carpathian region in extending the tephrostratigraphic framework to link between NW Europe and the eastern Mediterranean. There are several factors that could be responsible for the distal occurrences of the widespread ash from Iceland, Italy and Anatolia found in both records. The region of the Southern Carpathians is seasonally subjected to three major air circulation patterns originating from the Atlantic, the Mediterranean and with the influence of the Siberian High (Longman et al., 2017a, 2017b; Obreht et al., 2016). This atmospheric circulation pattern would result in the high potential of ash fall from the three different volcanic sources being deposited at the sites. The variable and constantly evolving weather patterns may have led to varying directions of ash plume dispersals from the different volcanic sources, resulting in patchy distribution of tephra identifications at sites across Europe (Jones et al., 2018). In addition, different atmospheric circulation patterns at varying elevations of ash plume heights from the associated eruptions may have resulted in divergent directions (Fisher, 1964). This could well be the case for the Anatolian tephra distribution to Lakes Lia and Brazi.

The resulting complex atmospheric circulations over Lakes Lia and Brazi have governed the distribution of ash fall from these different volcanic sources. It could be suggested that the dominance of tephra from a volcanic source potentially indicates the dominance of prevailing palaeo-wind directions, i.e. the presence of Italian tephra shows the influence of Mediterranean air masses (Bogaard and Schmincke, 1985). Geochemical analyses of cryptotephra shards from Lake Lia shows a higher occurrence of glass shards derived from Mediterranean volcanic eruptions compared to that is seen in Lake Brazi (Table 3). This may be due to the location of Lake Lia on the southern side of the Carpathian Mountains, where it is mainly influenced by the different air masses from the Mediterranean atmospheric circulation (Obreht et al., 2016; Longman et al., 2017a, 2017b).

A speculative factor for the identification of cryptotephra in Lakes Lia and Brazi records may have been the influence of the orography of the Carpathian Mountain range. The Carpathians rise up out of the low topography of central Europe forming a large barrier to atmospheric circulation. Turbulence caused by these mountains can influence the localised deposition of tephra transported within atmospheric circulation (Watt et al., 2015). In addition, orographic precipitation can enhance tephra deposition (Stevenson et al., 2013; Watt et al., 2015). The Retezat Mountains, where Lakes Lia and Brazi are located, is one of the wettest alpine regions in the Carpathian Mountains (Magyari et al., 2012; Obreht et al., 2016; Longman et al., 2017a, 2017b). Additional factors such as regional bias of cryptotephra investigations especially in south-eastern Europe (Watson et al., 2017), site-specific sedimentary taphonomic processes (Pyne-O'donnell, 2011) and lack of continuous high-resolution cryptotephra searches (Timms et al., 2017) may have all influenced the currently limited known spatial distribution of these tephrostratigraphic markers in other European records.

6. Conclusion

Building upon the work of Kearney et al. (2018) that identified the Askja-S tephra in Lakes Lia and Brazi, additional far-travelled volcanic glass shards have been identified and geochemically characterised using major, minor and trace element analysis. These cryptotephras are correlated to several volcanoes originating from three highly important volcanic centres and their volcanoes: 1) Iceland with Askja, Katla and Torfajokull; 2) Italy with Campi Flegrei, Ischia and Pantelleria and; 3) Anatolia with potential sources from Acigöl and/or Ericyles. Of these, three cryptotephra isochrons, in addition to the Askja-S, have been identified and dated in this study: 1) a LG Lipari tephra layer, identified in Lake Brazi (TDB_564); 2) an chrono-stratigraphic separate Early Holocene Lipari tephra (LIA_637) recorded in Lake Lia and; 3) an Early Holocene Ischia tephra traced in Lake Lia (LIA_612.5).

The use of trace element geochemical analysis was particularly successful in validating volcanic origins of high silica glass shards from either Iceland or Anatolia, in addition to confirmation of a LG Lipari tephra layer (Albert et al., 2017; McGuire et al., 2022). By using this combined geochemical analysis approach, there is future potential to discover additional/new important tephra layers as well as to refine the age of these distal tephras in other dated palaeoenvironmental records. These results show the importance of investigating distal records for volcanic ash to accurately understand past volcanic eruptive histories, particularly where there is no known proximal deposit or there is a current lack of geochemical data (i.e. Anatolia).

These important findings have highlighted the pivotal link that the Romanian palaeoenvironmental sites of Lake Brazi and Lia have within the wider European and Mediterranean tephra framework. Being uniquely located at the confluence of major atmospheric circulations and within proximity of several active volcanic centres, this region provides multiple opportunities to extend important tephrostratigraphic connections to numerous palaeoclimatic archives across the continent. This provides future opportunities to investigate the temporal and spatial environmental response of abrupt climatic changes from NW to SE Europe and beyond into the eastern Mediterranean, using tephra as a time synchronous marker during the LGIT.

Declaration of competing interest

The authors declare that they have no known competing financial interests or personal relationships that could have appeared to influence the work reported in this paper.

Data availability

Data is available as Supplementary material

Acknowledgements

RJK was funded by the UK National Environmental Research Council (NERC; grants: NE/L002612/1) as part of the Environmental Research Doctoral Training Program at the University of Oxford. PGA and RAS are supported by Early Career Fellowships from the Leverhulme Trust (grants: ECF-2014-438 and ECF-2015-396), while PGA has also been supported by a UKRI Future Leaders Fellowship (MR/S035478/1)'. The research was also supported by the National Multidisciplinary Laboratory for Climate Change, Hungary (NKFIH-471-3/2021, RRF-2.3.1-21-2022-00014), co-financed by the projects GINOP-2.3.2-15-2016-00019 and KKP 144209. AM was funded by a PhD studentship at the Department of Geography, University of Cambridge. Special thanks is given to Prof. Victoria Smith (Oxford, EPMA) and Dr. Christina Manning (RHUL, LA-ICP-MS) for their help with the analysis. The authors would like to

thank reviewers Biagio Giaccio and Sabine Wulf for their helpful comments and feedback.

Appendix A. Supplementary data

Supplementary data to this article can be found online at https://doi.org/10.1016/j.quascirev.2024.108558.

References

Albert, P.G., Hardiman, M., Keller, J., Tomlinson, E.L., Smith, V.C., Bourne, A.J., Wulf, S., Zanchetta, G., Sulpizio, R., Müller, U.C., Pross, J., Ottolini, L., Matthews, I. P., Blockley, S.P.E., Menzies, M.A., 2015. Revisiting the Y-3 tephrostratigraphic marker: a new diagnostic glass geochemistry, age estimate, and details on its climatostratigraphical context. Quat. Sci. Rev. 118, 105–121. https://doi.org/10.1016/j.quascirev.2014.04.002.

Albert, P.G., Tomlinson, E.L., Smith, V.C., Di Roberto, A., Todman, A., Rosi, M., Marani, M., Muller, W., Menzies, M.A., 2012. Marine-continental tephra correlations: volcanic glass geochemistry from the Marsili basin and the aeolian islands, southern Tyrrhenian Sea, Italy. J. Volcanol. Geoth. Res. 74–94. https://doi.org/10.1016/j.jvolgeores.2012.03.009, 229–230.

Albert, P.G., Tomlinson, E.L., Smith, V.C., Di Traglia, F., Pistolesi, M., Morris, A., Donato, P., De Rosa, R., Sulpizio, R., Keller, J., Rosi, M., Menzies, M., 2017. Glass geochemistry of pyroclastic deposits from the Aeolian Islands in the last 50 ka: a proximal database for tephrochronology. J. Volcanol. Geoth. Res. 336, 81–107. https://doi.org/10.1016/j.jvolgeores.2017.02.008.

Albert, P.G., Giaccio, B., Isaia, R., Costa, A., Niespolo, E.M., Nomade, S., Pereira, A., Renne, P.R., Hinchliffe, A., Mark, D.F., Brown, R.J., 2019. Evidence for a large-magnitude eruption from Campi Flegrei caldera (Italy) at 29 ka. Geology 47 (7), 595–599. https://doi.org/10.1130/G45805.1.

Bakke, J., Lie, O., Heegaard, E., Dokken, T., Haug, G.H., Birks, H.H., Dulski, P., Nilsen, T., 2009. Rapid oceanic and atmospheric changes during the Younger Dryas cold period. Nat. Geosci. 2, 202–205. https://doi.org/10.1038/ngeo439.

Barton, R.N.E., Lane, C.S., Albert, P.G., White, D., Collcutt, S.N., Bouzouggar, A., Ditchfield, P., Farr, L., Oh, A., Ottolini, L., Smith, V.C., Van Peer, P., Kindermann, K., 2015. The role of cryptotephra in refining the chronology of Late Pleistocene human evolution and cultural change in North Africa. Quat. Sci. Rev. 118, 151–169. https://doi.org/10.1016/j.quascirev.2014.09.008.

Bergman, J., Wastegård, S., Hammarlund, D., Wohlfarth, B., Roberts, S.J., 2004. Holocene tephra horizons at Klocka Bog, west-central Sweden: aspects of reproducibility in subarctic peat deposits. J. Quat. Sci. 19, 241–249. https://doi.org/10.1002/jqs.833.

Birks, H.H., Gulliksen, S., Haflidason, H., Mangerud, J., Possnert, G., 1996. New radiocarbon dates for the Vedde ash and the Saksunarvatn ash from western Norway. Quat Res 45, 119–127. https://doi.org/10.1006/qres.1996.0014.

Björck, S., Walker, M.J.C., Cwynar, L.C., Johnsen, S., Knudsen, K.-L., Lowe, J.J., Wohlfarth, B., 1998. An event stratigraphy for the Last Termination in the North Atlantic region based on the Greenland ice-core record: a proposal by the INTIMATE group. J. Quat. Sci. 13, 283–292. https://doi.org/10.1002/(SICI)1099-1417(199807/08)13:4<283::AID-JQS386>3.0.CO;2-A.

Blaauw, M., 2012. Out of tune: the dangers of aligning proxy archives. Quat. Sci. Rev. 36, 38–49. https://doi.org/10.1016/j.quascirev.2010.11.012.

Blockley, S.P.E., Lane, C.S., Lotter, A.F., Pollard, A.M., 2007. Evidence for the presence of the Vedde ash in central Europe. Quat. Sci. Rev. 26, 3030–3036. https://doi.org/10.1016/j.quascirev.2007.09.010.

Blockley, S.P.E., Pyne-O'Donnell, S.D.F., Lowe, J.J., Matthews, I.P., Stone, A., Pollard, A. M., Turney, C.S.M., Molyneux, E.G., 2005. A new and less destructive laboratory procedure for the physical separation of distal glass tephra shards from sediments. Quat. Sci. Rev. 24, 1952–1960. https://doi.org/10.1016/j.quascirev.2004.12.008.

Blockley, S., Pellegrini, M., Colonese, A.C., Vetro, D.L., Albert, P.G., Brauer, A., Di Giuseppe, Z., Evans, A., Harding, P., Lee-Thorp, J., Lincoln, P., 2018. Dating human occupation and adaptation in the southern European last glacial refuge: the chronostratigraphy of Grotta del Romito (Italy). Quat. Sci. Rev. 184, 5–25. https://doi.org/10.1016/j.quascirev.2017.09.007.

Bogaard, P.v. d., Schmincke, H., 1985. Laacher See Tephra: a widespread isochronous late Quaternary tephra layer in central and northern Europe. Geol. Soc. Am. Bull. 96, 1554. https://doi.org/10.1130/0016-7606(1985)96<1554:LSTAWI>2.0.CO;2.

Bond, G.C., Mandeville, C., Hoffmann, S., 2001. Were rhyolitic glasses in the Vedde Ash and in the North Atlantic's Ash Zone 1 produced by the same volcanic eruption? Quat. Sci. Rev. 20, 1189–1199. https://doi.org/10.1016/S0277-3791(00)00146-3.

Bourne, A.J., Lowe, J.J., Trincardi, F., Asioli, A., Blockley, S.P.E., Wulf, S., Matthews, I. P., Piva, A., Vigliotti, L., 2010. Distal tephra record for the last ca 105,000 years from core PRAD 1-2 in the central Adriatic Sea: implications for marine tephrostratigraphy. Quat. Sci. Rev. 29, 3079–3094. https://doi.org/10.1016/j.quascirev.2010.07.021.

Brauer, A., Hajdas, I., Blockley, S.P.E., Bronk Ramsey, C., Christl, M., Ivy-Ochs, S., Moseley, G.E., Nowaczyk, N.N., Rasmussen, S.O., Roberts, H.M., Spötl, C., Staff, R. A., Svensson, A., 2014. The importance of independent chronology in integrating records of past climate change for the 60-8ka INTIMATE time interval. Quat. Sci. Rev. 106, 47–66. https://doi.org/10.1016/j.quascirev.2014.07.006.

Bronk Ramsey, C., 2009. Bayesian analysis of radiocarbon dates. Radiocarbon 51, 337–360. https://doi.org/10.1017/s0033822200033865.

Bronk Ramsey, C., 2008. Deposition models for chronological records. Quat. Sci. Rev. 27, 42–60. https://doi.org/10.1016/j.quascirev.2007.01.019.

Bronk Ramsey, C., Albert, P., Blockley, S., Hardiman, M., Lane, C., Macleod, A., Matthews, I.P., Muscheler, R., Palmer, A., Staff, R.A., 2014. Integrating timescales with time-transfer functions: a practical approach for an INTIMATE database. Quat. Sci. Rev. 106, 67–80. https://doi.org/10.1016/j.quascirev.2014.05.028.

Bronk Ramsey, C., Albert, P.G., Blockley, S.P.E., Hardiman, M., Housley, R.A., Lane, C.S., Lee, S., Matthews, I.P., Smith, V.C., Lowe, J.J., 2015. Improved age estimates for key Late Quaternary European tephra horizons in the RESET lattice. Quat. Sci. Rev. 118, 18–32. https://doi.org/10.1016/j.quascirev.2014.11.007.

Bronk Ramsey, C., Lee, S., 2013. Recent and planned developments of the Program OxCal. Radiocarbon 55, 720–730. https://doi.org/10.1017/s0033822200057878.

Buczkó, K., Magyari, E.K., Soróczki-Pintér, É., Hubay, K., Braun, M., Bálint, M., 2009. Diatom-based evidence for abrupt climate changes during the late glacial in the southern Carpathian mountains. Central European Geology 52, 249–268. https://doi.org/10.1556/CEuGeol.52.2009.3-4.3.

Caron, B., Siani, G., Sulpizio, R., Zanchetta, G., Paterne, M., Santacroce, R., Tema, E., Zanella, E., 2012. Late Pleistocene to Holocene tephrostratigraphic record from the northern Ionian Sea. Mar Geol 311– 314, 41–51. https://doi.org/10.1016/j.margeo.2012.04.001.

Cassidy, M., Watt, S.F.L., Palmer, M.R., Trofimovs, J., Symons, W., Maclachlan, S.E., Stinton, A.J., 2014. Construction of volcanic records from marine sediment cores: a review and case study (Montserrat, West Indies). Earth Sci. Rev. 138, 137–155. https://doi.org/10.1016/j.earscirev.2014.08.008.

Civetta, L., Cornette, Y., Gillot, P.Y., Orsi, G., 1988. The eruptive history of Pantelleria (Sicily channel) in the last 50 ka. Bull. Volcanol. 50, 47–57. https://doi.org/10.1007/BF01047508.

Civetta, L., Gallo, G., Orsi, G., 1991. Sr-and Nd-isotope and trace-element constraints on the chemical evolution of the magmatic system of Ischia (Italy) in the last 55 ka. J. Volcanol. Geoth. Res. 46, 213–230.

Clark, P.U., Marshall, S.J., Clarke, G.K.C., Hostetler, S.W., Licciardi, J.M., Teller, J.T., 2001. Freshwater forcing of abrupt climate change during the last glaciation. Science 293 (1979), 283–287. https://doi.org/10.1126/science.1062517.

Cook, E., Davies, S.M., Guðmundsdóttir, E.R., Abbott, P.M., Pearce, N.J.G., 2018. First identification and characterization of Borrobol-type tephra in the Greenland ice cores: new deposits and improved age estimates. J. Quat. Sci. 33, 212–224. https://doi.org/10.1002/jqs.3016.

Cullen, V.L., Smith, V.C., Arz, H.W., 2014. The detailed tephrostratigraphy of a core from the south-east Black Sea spanning the last ~60 ka. J. Quat. Sci. 29, 675–690. https://doi.org/10.1002/jqs.2739.

Davies, S., 2015. Cryptotephras: the revolution in correlation and precision dating. J. Quat. Sci. 30, 114–130. https://doi.org/10.1002/jqs.2766.

Davies, S.M., Abbott, P.M., Pearce, N.J.G., Wastegård, S., Blockley, S.P.E., 2012. Integrating the INTIMATE records using tephrochronology: rising to the challenge. Quat. Sci. Rev. 36, 11–27. https://doi.org/10.1016/j.quascirev.2011.04.005.

Davies, S.M., Elmquist, M., Bergman, J., Wohlfarth, B., Hammarlund, D., 2007. Cryptotephra sedimentation processes within two lacustrine sequences from west central Sweden. Holocene 17, 319–330. https://doi.org/10.1177/0959683607076443.

Davies, S.M., Hoak, W.Z., Bohncke, S.J.P., Lowe, J.J., Pyne-O'Donnell, S., Turney, C.S. M., 2005. Detection of Lateglacial distal tephra layers in The Netherlands. Boreas 34, 123–135. https://doi.org/10.1111/j.1502-3885.2005.tb01010.x.

Davies, S.M., Wastegård, S., Wohlfarth, B., 2003. Extending the limits of the Borrobol Tephra to Scandinavia and detection of new early Holocene tephras. Quat Res 59, 345–352. https://doi.org/10.1016/S0033-5894(03)00035-8.

de Vita, S., Sansivero, F., Orsi, G., Marotta, E., 2006. Cyclical slope instability and volcanism related to volcano-tectonism in resurgent calderas: the Ischia island (Italy) case study. Eng. Geol. 86, 148–165. https://doi.org/10.1016/j.enggeo.2006.02.013.

Eastwood, W.J., Pearce, N.J.G., Westgate, J.A., Perkins, W.T., Lamb, H.F., Roberts, N., 1999. Geochemistry of Santorini tephra in lake sediments from Southwest Turkey. Glob Planet Change 21, 17–29. https://doi.org/10.1016/S0921-8181(99)00005-3.

Finsinger, W., Fevre, J., Orbán, I., Pál, I., Vincze, I., Hubay, K., Birks, H.H., Braun, M., Tóth, M., Magyari, E.K., 2018. Holocene fire-regime changes near the treeline in the Retezat Mts. (southern Carpathians, Romania). Quat. Int. 477, 94–105. https://doi.org/10.1016/j.quaint.2016.04.029.

Fisher, R.V., 1964. Maximum size, median diameter, and sorting of tephra. J. Geophys. Res. 69, 341–355. https://doi.org/10.1029/JZ069i002p00341.

Forni, F., Lucchi, F., Peccerillo, A., Tranne, C.A., Rossi, P.L., Frezzotti, M.L., 2013. Stratigraphy and geological evolution of the lipari volcanic complex (central aeolian archipelago). Geological Society Memoir 37, 213–279. https://doi.org/10.1144/M37.10.

Gudmundsdóttir, E.R., Larsen, G., Björck, S., Ingólfsson, Ó., Striberger, J., 2016. A new high-resolution Holocene tephra stratigraphy in eastern Iceland: improving the Icelandic and North Atlantic tephrochronology. Quat. Sci. Rev. 150, 234–249. https://doi.org/10.1016/j.quascirev.2016.08.011.

Haflidason, H., Regnéll, C., Pyne-O'Donnell, S., Svendsen, J.I., 2019. Extending the known distribution of the Vedde ash into Siberia: occurrence in Lake sediments from the timan ridge and the Ural mountains, northern Russia. Boreas 48, 444–451. https://doi.org/10.1111/bor.12354.

Haliuc, A., Veres, D., Brauer, A., Hubay, K., Hutchinson, S., Begy, R., Braun, M., 2017. Palaeohydrological changes during the mid and late Holocene in the Carpathian area, central-eastern Europe. Glob Planet Change 152, 99–114. https://doi.org/10.1016/j.gloplacha.2017.02.010.

Hamann, Y., Wulf, S., Ersoy, O., Ehrmann, W., Aydar, E., Schmiedl, G., 2010. First evidence of a distal early Holocene ash layer in Eastern Mediterranean deep-sea

sediments derived from the Anatolian volcanic province. Quat Res 73, 497–506. https://doi.org/10.1016/j.yqres.2009.12.004.
Harangi, S., Molnár, K., Schmitt, A.K., Dunkl, I., Seghedi, I., Novothny, Á., Molnár, M., Kiss, B., Ntaflos, T., Mason, P.R.D., Lukács, R., 2020. Fingerprinting the late Pleistocene tephras of Ciomadul volcano, eastern–central Europe. J. Quat. Sci. 35, 232–244. https://doi.org/10.1002/jqs.3177.
Harning, D.J., Thordarson, T., Geirsdóttir, Á., Zalzal, K., Miller, G.H., 2018. Provenance, stratigraphy and chronology of Holocene tephra from Vestfirðir, Iceland. Quat. Geochronol. 46, 59–76. https://doi.org/10.1016/j.quageo.2018.03.007.
Housley, R.A., MacLeod, A., Nalepka, D., Jurochnik, A., Masojć, M., Davies, L., Lincoln, P.C., Bronk Ramsey, C., Gamble, C.S., Lowe, J.J., 2013. Tephrostratigraphy of a Lateglacial lake sediment sequence at Węgliny, southwest Poland. Quat. Sci. Rev. 77, 4–18. https://doi.org/10.1016/j.quascirev.2013.07.014.
Hubay, K., Molnár, M., Orbán, I., Braun, M., Bíró, T., Magyari, E., 2018. Age–depth relationship and accumulation rates in four sediment sequences from the Retezat Mts, South Carpathians (Romania). Quat. Int. 477, 7–18. https://doi.org/10.1016/j.quaint.2016.09.019.
Hunt, J.B., 1994. The mobility and redeposition of the Hekla 1991 tephra, and the effects of wind and snow. In: Stötter, J., Wilhelm, F. (Eds.), Environmental Change in Iceland. Münchener Geographische Abhandlungen, pp. 157–175.
Hunt, J.B., Hill, P.G., 1996. An inter-laboratory comparison of the Electron Probe Microanalysis of glass geochemistry. Quat. Int. 229–241.
Jancsik, P., 2001. A Retyezát-hegység (the Retezat mountains). Pallas–Akadémia Könyvkiadó 140.
Jochum, K.P., Stoll, B., Herwig, K., Willbold, M., Hofmiann, A.W., Amini, M., Aarburg, S., Abouchami, W., Hellebrand, E., Mocek, B., Raczek, I., Stracke, A., Alard, O., Bouman, C., Becker, S., Dücking, M., Brätz, H., Klemd, R., De Bruin, D., Canil, D., Cornell, D., De Hoog, C.J., Dalpé, C., Danyushevshy, L., Eisenhauer, A., Gao, Y., Snow, J.E., Groschopf, N., Günther, D., Latkoczy, C., Guillong, M., Hauri, E.H., Höfer, H.E., Lahaye, Y., Horz, K., Jacob, D.E., Kasemann, S.A., Kent, A.J.R., Ludwig, T., Zack, T., Mason, P.R.D., Meixner, A., Rosner, M., Misawa, K., Nash, B.P., Pfänder, J., Premo, W.R., Sun, W.D., Tiepolo, M., Vannucci, R., Vennemann, T., Wayne, D., Woodhead, J.D., 2006. MPI-DING reference glasses for in situ microanalysis: new reference values for element concentrations and isotope ratios. G-cubed 7. https://doi.org/10.1029/2005GC001060.
Jóhannsdöttir, G., 2007. Mid Holocene to Late Glacial Tephrochronology in West Iceland as Revealed in Three Lacustrine Environments. University of Iceland. MSc Thesis in Geology.
Jones, G., Davies, S.M., Farr, G.J., Bevan, J., 2017. Identification of the Askja-S tephra in a rare turlough record from Pant-y-Llyn, south Wales. PGA (Proc. Geol. Assoc.) 128, 523–530. https://doi.org/10.1016/j.pgeola.2017.05.010.
Jones, G., Lane, C.S., Brauer, A., Davies, S.M., de Bruijn, R., Engels, S., Haliuc, A., Hoek, W.Z., Merkt, J., Sachse, D., Turner, F., Wagner-Cremer, F., 2018. The Lateglacial to early Holocene tephrochronological record from Lake Hämelsee, Germany: a key site within the European tephra framework. Boreas 47, 28–40. https://doi.org/10.1111/bor.12250.
Karátson, D., Wulf, S., Veres, D., Magyari, E.K., Gertisser, R., Timar-Gabor, A., Novothny, Á., Telbisz, T., Szalai, Z., Anechitei-Deacu, V., Appelt, O., Bormann, M., Jánosi, Cs, Hubay, K., Schäbitz, F., 2016. The latest explosive eruptions of Ciomadul (Csomád) volcano, East Carpathians — a tephrostratigraphic approach for the 51–29 ka BP time interval. J. Volcanol. Geoth. Res. 319, 29–51. https://doi.org/10.1016/j.jvolgeores.2016.03.005.
Karkanas, P., White, D., Lane, C.S., Stringer, C., Davies, W., Cullen, V.L., Smith, V.C., Ntinou, M., Tsartsidou, G., Kyparissi-Apostolika, N., 2015. Tephra correlations and climatic events between the MIS6/5 transition and the beginning of MIS3 in Theopetra Cave, central Greece. Quat. Sci. Rev. 118, 170–181. https://doi.org/10.1016/j.quascirev.2014.05.027.
Kearney, R., Albert, P.G., Staff, R.A., Pál, I., Veres, D., Magyari, E., Bronk Ramsey, C., 2018. Ultra-distal fine ash occurrences of the Icelandic Askja-S Plinian eruption deposits in Southern Carpathian lakes: new age constraints on a continental scale tephrostratigraphic marker. Quat. Sci. Rev. 188, 174–182. https://doi.org/10.1016/j.quascirev.2018.03.035.
Kelly, T.J., Hardiman, M., Lovelady, M., Lowe, J.J., Matthews, I.P., Blockley, S.P.E., 2017. Scottish early Holocene vegetation dynamics based on pollen and tephra records from Inverlair and Loch Etteridge, Inverness-shire. PGA (Proc. Geol. Assoc.) 128, 125–135. https://doi.org/10.1016/j.pgeola.2016.02.008.
Kwiecien, O., Arz, H.W., Lamy, F., Wulf, S., Bahr, A., Röhl, U., Haug, G.H., 2008. Estimated reservoir ages of the black sea since the last glacial. Radiocarbon 50, 99–118. https://doi.org/10.1017/S0033822200043393.
Lane, C.S., Blockley, S.P.E., Bronk Ramsey, C., Lotter, A.F., 2011a. Tephrochronology and absolute centennial scale synchronisation of European and Greenland records for the last glacial to interglacial transition: a case study of Soppensee and NGRIP. Quat. Int. 246, 145–156. https://doi.org/10.1016/j.quaint.2010.11.028.
Lane, C.S., Andrič, M., Cullen, V.L., Blockley, S.P.E., 2011b. The occurrence of distal Icelandic and Italian tephra in the Lateglacial of Lake Bled, Slovenia. Quat. Sci. Rev. 30, 1013–1018. https://doi.org/10.1016/j.quascirev.2011.02.014.
Lane, C.S., De Klerk, P., Cullen, V.L., 2012a. A tephrochronology for the Lateglacial palynological record of the Endinger Bruch (Vorpommern, north-east Germany). J. Quat. Sci. 27, 141–149. https://doi.org/10.1002/jqs.1521.
Lane, C.S., Blockley, S.P.E., Lotter, A.F., Finsinger, W., Filippi, M.L., Matthews, I.P., 2012b. A regional tephrostratigraphic framework for central and southern European climate archives during the Last Glacial to Interglacial transition: comparisons north and south of the Alps. Quat. Sci. Rev. 36, 50–58. https://doi.org/10.1016/j.quascirev.2010.10.015.
Lane, C.S., Blockley, S.P.E., Mangerud, J., Smith, V.C., Lohne, Ø.S., Tomlinson, E.L., Matthews, I.P., Lotter, A.F., 2012c. Was the 12.1ka Icelandic Vedde ash one of a kind? Quat. Sci. Rev. 33, 87–99. https://doi.org/10.1016/j.quascirev.2011.11.011.
Lane, C.S., Brauer, A., Blockley, S.P.E., Dulski, P., 2013. Volcanic ash reveals time-transgressive abrupt climate change during the Younger Dryas. Geology 41, 1251–1254. https://doi.org/10.1130/G34867.1.
Lane, C.S., Brauer, A., Martín-Puertas, C., Blockley, S.P.E., Smith, V.C., Tomlinson, E.L., 2015. The Late Quaternary tephrostratigraphy of annually laminated sediments from Meerfelder Maar, Germany. Quat. Sci. Rev. 122, 192–206. https://doi.org/10.1016/j.quascirev.2015.05.025.
Lane, C.S., Cullen, V.L., White, D., Bramham-Law, C.W.F., Smith, V.C., 2014. Cryptotephra as a dating and correlation tool in archaeology. J. Archaeol. Sci. 42, 42–50. https://doi.org/10.1016/j.jas.2013.10.033.
Larsen, J.J., Noe-Nygaard, N., 2014. Lateglacial and early Holocene tephrostratigraphy and sedimentology of the Store Slotseng basin, SW Denmark: a multi-proxy study. Boreas 43, 349–361. https://doi.org/10.1111/bor.12040.
Lawson, I., Frogley, M., Bryant, C., Preece, R., Tzedakis, P., 2004. The Lateglacial and Holocene environmental history of the Ioannina basin, north-west Greece. Quat. Sci. Rev. 23, 1599–1625. https://doi.org/10.1016/j.quascirev.2004.02.003.
Le Bas, M.J., Le Maitre, R.W., Streckeisen, A., Zanettin, B., 1986. A chemical classification of volcanic rocks based on the total alkali-silica diagram. J. Petrol. 27, 745–750.
Lilja, C., Lind, E.M., Morén, B., Wastegård, S., 2013. A lateglacial-early Holocene tephrochronology for SW Sweden. Boreas 42, 544–554. https://doi.org/10.1111/j.1502-3885.2012.00296.x.
Lind, E.M., Lilja, C., Wastegård, S., Pearce, N.J.G., 2016. Revisiting the Borrobol tephra. Boreas 45, 629–643. https://doi.org/10.1111/bor.12176.
Lind, E.M., Wastegård, S., 2011. Tephra horizons contemporary with short early Holocene climate fluctuations: new results from the Faroe Islands. Quat. Int. 246, 157–167. https://doi.org/10.1016/j.quaint.2011.05.014.
Longman, J., Ersek, V., Veres, D., Salzmann, U., 2017a. Detrital events and hydroclimate variability in the Romanian Carpathians during the mid-to-late Holocene. Quat. Sci. Rev. 167, 78–95. https://doi.org/10.1016/j.quascirev.2017.04.029.
Longman, J., Veres, D., Ersek, V., Salzmann, U., Hubay, K., Bormann, M., Wennrich, V., Schäbitz, F., 2017b. Periodic input of dust over the Eastern Carpathians during the Holocene linked with Saharan desertification and human impact. Clim. Past 13, 897–917. https://doi.org/10.5194/cp-13-897-2017.
Lowe, D.J., 2011. Tephrochronology and its application: a review. Quat. Geochronol. 6, 107–153. https://doi.org/10.1016/j.quageo.2010.08.003.
Lowe, J.J., Blockley, S., Trincardi, F., Asioli, A., Cattaneo, A., Matthews, I.P., Pollard, M., Wulf, S., 2007. Age modelling of late Quaternary marine sequences in the Adriatic: towards improved precision and accuracy using volcanic event stratigraphy. Continent. Shelf Res. 27, 560–582. https://doi.org/10.1016/j.csr.2005.12.017.
Lowe, J.J., Palmer, A.P., Carter-Champion, A., MacLeod, A., Ramírez-Rojas, I., Timms, R.G.O., 2017. Stratigraphy of a Lateglacial lake basin sediment sequence at Turret bank, upper glen Roy, Lochaber: implications for the age of the Turret fan. PGA (Proc. Geol. Assoc.) 128, 110–124. https://doi.org/10.1016/j.pgeola.2016.12.008.
Lowe, J.J., Ramsey, C.B., Housley, R.A., Lane, C.S., Tomlinson, E.L., 2015. RESET Associates and RESET team. In: The RESET Project: Constructing a European Tephra Lattice for Refined Synchronisation of Environmental and Archaeological Events during the Last C. 100 Ka. Quat Sci Rev, vol. 118, pp. 1–17. https://doi.org/10.1016/j.quascirev.2015.04.006.
Lowe, J.J., Rasmussen, S.O., Björck, S., Hoek, W.Z., Steffensen, J.P., Walker, M.J.C., Yu, Z.C., 2008. Synchronisation of palaeoenvironmental events in the North Atlantic region during the Last Termination: a revised protocol recommended by the INTIMATE group. Quat. Sci. Rev. 27, 6–17. https://doi.org/10.1016/j.quascirev.2007.09.016.
MacDonald, R., 1974. Nomenclature and petrochemistry of the peralkaline oversaturated extrusive rocks. Bull. Volcanol. 38, 498–516. https://doi.org/10.1007/BF02596896.
MacLeod, A., Matthews, I.P., Lowe, J.J., Palmer, A.P., Albert, P.G., 2015. A second tephra isochron for the Younger Dryas period in northern Europe: the Abernethy Tephra. Quat. Geochronol. 28, 1–11. https://doi.org/10.1016/j.quageo.2015.03.010.
Magny, M., de Beaulieu, J.-L., Drescher-Schneider, R., Vannière, B., Walter-Simonnet, A.-V., Millet, L., Bossuet, G., Peyron, O., 2006. Climatic oscillations in central Italy during the last glacial–Holocene transition: the record from Lake Accesa. J. Quat. Sci. 21, 311–320. https://doi.org/10.1002/jqs.999.
Magny, M., Vannière, B., Calo, C., Millet, L., Leroux, A., Peyron, O., Zanchetta, G., La Mantia, T., Tinner, W., 2011. Holocene hydrological changes in south-western Mediterranean as recorded by lake-level fluctuations at Lago Preola, a coastal lake in southern Sicily, Italy. Quat. Sci. Rev. 30, 2459–2475. https://doi.org/10.1016/j.quascirev.2011.05.018.
Magyari, Braun, Buczkó, Kern, László, Hubay, Bálint, 2009. Radiocarbon chronology of glacial lake sediments in the Retezat Mts (South Carpathians, Romania): a window to Late Glacial and Holocene climatic and paleoenvironmental changes. Central European Geology 52, 225–248. https://doi.org/10.1556/CEuGeol.52.2009.3-4.2.
Magyari, E., Jakab, G., Braun, M., Buczkó, K., Bálint, M., 2009. High-resolution study of late glacial and early Holocene vegetation and tree line changes in the southern Carpathian mountains. Geophys. Res. Abstr. 11, 2009–10549.
Magyari, E., Vincze, I., Orbán, I., Bíró, T., Pál, I., 2018. Timing of major forest compositional changes and tree expansions in the Retezat Mts during the last 16,000 years. Quat. Int. 477, 40–58. https://doi.org/10.1016/j.quaint.2017.12.054.
Magyari, E.K., Jakab, G., Bálint, M., Kern, Z., Buczkó, K., Braun, M., 2012. Rapid vegetation response to Lateglacial and early Holocene climatic fluctuation in the south Carpathian mountains (Romania). Quat. Sci. Rev. 35, 116–130. https://doi.org/10.1016/j.quascirev.2012.01.006.

Mahood, G.A., Hildreth, W., 1986. Geology of the peralkaline volcano at Pantelleria, strait of Sicily. Bull. Volcanol. 48, 143–172. https://doi.org/10.1007/BF01046548.
Margari, V., Pyle, D.M., Bryant, C., Gibbard, P.L., 2007. Mediterranean tephra stratigraphy revisited: results from a long terrestrial sequence on Lesvos Island, Greece. J. Volcanol. Geoth. Res. 163, 34–54. https://doi.org/10.1016/j.jvolgeores.2007.02.002.
Matthews, I.P., Birks, H.H., Bourne, A.J., Brooks, S.J., Lowe, J.J., MacLeod, A., Pyne-O'Donnell, S.D.F., 2011. New age estimates and climatostratigraphic correlations for the Borrobol and Penifiler tephras: evidence from Abernethy forest, Scotland. J. Quat. Sci. 26, 247–252. https://doi.org/10.1002/jqs.1498.
Matthews, I.P., Trincardi, F., Lowe, J.J., Bourne, A.J., MacLeod, A., Abbott, P.M., Andersen, N., Asioli, A., Blockley, S.P.E., Lane, C.S., Oh, Y.A., 2015. Developing a robust tephrochronological framework for Late Quaternary marine records in the Southern Adriatic Sea: new data from core station SA03-11. Quat. Sci. Rev. 118, 84–104. https://doi.org/10.1016/j.quascirev.2014.10.009.
McGuire, A.M., Lane, C.S., Roucoux, K.H., Albert, P.G., Kearney, R., 2022. The dating and correlation of an eastern Mediterranean lake sediment sequence: a 46–4 ka tephrostratigraphy for Ioannina (NW Greece). J. Quat. Sci. 37, 1313–1331. https://doi.org/10.1002/jqs.3452.
Moles, J.D., McGarvie, D., Stevenson, J.A., Sherlock, S.C., Abbott, P.M., Jenner, F.E., Halton, A.M., 2019. Widespread tephra dispersal and ignimbrite emplacement from a subglacial volcano (Torfajökull, Iceland). Geology 47, 577–580. https://doi.org/10.1130/G46004.1.
Muschitiello, F., Wohlfarth, B., 2015. Time-transgressive environmental shifts across northern Europe at the onset of the younger Dryas. Quat. Sci. Rev. 109, 49–56. https://doi.org/10.1016/j.quascirev.2014.11.015.
Neave, D.A., Fabbro, G., Herd, R.A., Petrone, C.M., Edmonds, M., 2012. Melting, Differentiation and Degassing at the Pantelleria volcano, Italy. J. Petrol. 53, 637–663. https://doi.org/10.1093/petrology/egr074.
Negri, A., Capotondi, L., Keller, J., 1999. Calcareous nannofossils, planktonic foraminifera and oxygen isotopes in the late Quaternary sapropels of the Ionian Sea. Mar. Geol. 157, 89–103. https://doi.org/10.1016/S0025-3227(98)00135-2.
Neugebauer, I., Müller, D., Schwab, M.J., Blockley, S., Lane, C.S., Wulf, S., Appelt, O., Brauer, A., 2021. Cryptotephras in the Lateglacial ICDP Dead Sea sediment record and their implications for chronology. Boreas 50, 844–861. https://doi.org/10.1111/bor.12516.
Neugebauer, I., Wulf, S., Schwab, M.J., Serb, J., Plessen, B., Appelt, O., Brauer, A., 2017. Implications of S1 tephra findings in Dead Sea and Tayma palaeolake sediments for marine reservoir age estimation and palaeoclimate synchronisation. Quat. Sci. Rev. 170, 269–275. https://doi.org/10.1016/j.quascirev.2017.06.020.
Ntinou, M., Kyparissi-Apostolika, N., 2016. Local vegetation dynamics and human habitation from the last interglacial to the early Holocene at Theopetra cave, central Greece: the evidence from wood charcoal analysis. Veg. Hist. Archaeobotany 25, 191–206. https://doi.org/10.1007/s00334-015-0538-7.
Obreht, I., Hambach, U., Veres, D., Zeeden, C., Bösken, J., Stevens, T., Marković, S.B., Klasen, N., Brill, D., Burow, C., Lehmkuhl, F., 2017. Shift of large-scale atmospheric systems over Europe during late MIS 3 and implications for Modern Human dispersal. Sci. Rep. 7 https://doi.org/10.1038/s41598-017-06285-x.
Obreht, I., Zeeden, C., Hambach, U., Veres, D., Marković, S.B., Bösken, J., Svirčev, Z., Bačević, N., Gavrilov, M.B., Lehmkuhl, F., 2016. Tracing the influence of Mediterranean climate on Southeastern Europe during the past 350,000 years. Sci. Rep. 6 https://doi.org/10.1038/srep36334.
Orsi, G., De Vita, S., Di Vito, M., 1996. The restless, resurgent Campi Flegrei nested caldera (Italy): constraints on its evolution and configuration. J. Volcanol. Geoth. Res. 74 (3–4), 179–214. https://doi.org/10.1016/S0377-0273(96)00063-7.
Pál, I., Buczkó, K., Vincze, I., Finsinger, W., Braun, M., Biró, T., Magyari, E.K., 2018. Terrestrial and aquatic ecosystem responses to early Holocene rapid climate change (RCC) events in the South Carpathian Mountains, Romania. Quat. Int. 477, 79–93. https://doi.org/10.1016/j.quaint.2016.11.015.
Pappalardo, L., Civetta, L., D'Antonio, M., Deino, A., Di Vito, M., Orsi, G., Carandente, A., de Vita, S., Isaia, R., Piochi, M., 1999. Chemical and Sr-isotopical evolution of the phlegraean magmatic system before the campanian ignimbrite and the neapolitan Yellow Tuff eruptions. J. Volcanol. Geoth. Res. 91 (2–4), 141–166. https://doi.org/10.1016/S0377-0273(99)00033-5.
Paterne, M., Guichard, F., Duplessy, J.C., Siani, G., Sulpizio, R., Labeyrie, J., 2008. A 90,000-200,000 yrs marine tephra record of Italian volcanic activity in the Central Mediterranean Sea. J. Volcanol. Geoth. Res. 177, 187–196. https://doi.org/10.1016/j.jvolgeores.2007.11.028.
Paterne, M., Guichard, F., Labeyrie, J., 1988. Explosive activity of the South Italian volcanoes during the past 80,000 years as determined by marine tephrochronology. J. Volcanol. Geoth. Res. 34, 153–172. https://doi.org/10.1016/0377-0273(88)90030-3.
Pearce, J.A., Bender, J.F., De Long, S.E., Kidd, W.S.F., Low, P.J., Güner, Y., Saroglu, F., Yilmaz, Y., Moorbath, S., Mitchell, J.G., 1990. Genesis of collision volcanism in eastern Anatolia, Turkey. J. Volcanol. Geoth. Res. https://doi.org/10.1016/0377-0273(90)90018-B.
Peccerillo, A., Taylor, S.R., 1976. Geochemistry of Eocene calc-alkaline volcanic rocks from the Kastamonu area, northern Turkey. Contrib. Mineral. Petrol. 58, 63–81.
Pilcher, J., Bradley, R., Francus, P., Anderson, L., 2005. A Holocene tephra record from the lofoten islands, arctic Norway. Boreas 34, 136–156. https://doi.org/10.1080/03009480510012935.
Plunkett, G., Pilcher, J.R., 2018. Defining the potential source region of volcanic ash in northwest Europe during the Mid- to Late Holocene. Earth Sci. Rev. 179, 20–37. https://doi.org/10.1016/j.earscirev.2018.02.006.
Pyne-O'donnell, S., 2011. The taphonomy of Last Glacial-Interglacial Transition (LGIT) distal volcanic ash in small Scottish lakes. Boreas 40, 131–145. https://doi.org/10.1111/j.1502-3885.2010.00154.x.
Pyne-O'Donnell, S.D.F., 2007. Three new distal tephras in sediments spanning the last glacial–interglacial transition in scotland. J. Quat. Sci. 22, 559–570. https://doi.org/10.1002/jqs.1066.
Pyne-O'Donnell, S.D.F., Blockley, S.P.E., Turney, C.S.M., Lowe, J.J., 2008. Distal volcanic ash layers in the Lateglacial Interstadial (GI-1): problems of stratigraphic discrimination. Quat. Sci. Rev. 27, 72–84. https://doi.org/10.1016/j.quascirev.2007.02.019.
Pyne-O'Donnell, S.D.F., Jensen, B.J.L., 2020. Glacier Peak and mid-Lateglacial Katla cryptotephras in Scotland: potential new intercontinental and marine-terrestrial correlations. J. Quat. Sci. 35, 155–162. https://doi.org/10.1002/jqs.3171.
Ram, M., Donarummo, J., Sheridan, M., 1996. Volcanic ash from Icelandic ~57,300 Yr BP eruption found in GISP2 (Greenland) Ice Core. Geophys. Res. Lett. 23, 3167–3169. https://doi.org/10.1029/96GL03099.
Rasmussen, S.O., Andersen, K.K., Svensson, A.M., Steffensen, J.P., Vinther, B.M., Clausen, H.B., Siggaard-Andersen, M.L., Johnsen, S.J., Larsen, L.B., Dahl-Jensen, D., Bigler, M., Röthlisberger, R., Fischer, H., Goto-Azuma, K., Hansson, M.E., Ruth, U., 2006. A new Greenland ice core chronology for the last glacial termination. J. Geophys. Res. Atmos. 111 https://doi.org/10.1029/2005JD006079.
Rasmussen, S.O., Bigler, M., Blockley, S.P., Blunier, T., Buchardt, S.L., Clausen, H.B., Cvijanovic, I., Dahl-Jensen, D., Johnsen, S.J., Fischer, H., Gkinis, V., Guillevic, M., Hoek, W.Z., Lowe, J.J., Pedro, J.B., Popp, T., Seierstad, I.K., Steffensen, J.P., Svensson, A.M., Vallelonga, P., Vinther, B.M., Walker, M.J.C., Wheatley, J.J., Winstrup, M., 2014. A stratigraphic framework for abrupt climatic changes during the Last Glacial period based on three synchronized Greenland ice-core records: refining and extending the INTIMATE event stratigraphy. Quat. Sci. Rev. 106, 14–28. https://doi.org/10.1016/j.quascirev.2014.09.007.
Reimer, P.J., Austin, W.E.N., Bard, E., Bayliss, A., Blackwell, P.G., Bronk Ramsey, C., Butzin, M., Cheng, H., Edwards, R.L., Friedrich, M., Grootes, P.M., Guilderson, T.P., Hajdas, I., Heaton, T.J., Hogg, A.G., Hughen, K.A., Kromer, B., Manning, S.W., Muscheler, R., Palmer, J.G., Pearson, C., Van Der Plicht, J., Reimer, R.W., Richards, D.A., Scott, E.M., Southon, J.R., Turney, C.S.M., Wacker, L., Adolphi, F., Büntgen, U., Capano, M., Fahrni, S.M., Fogtmann-Schulz, A., Friedrich, R., Köhler, P., Kudsk, S., Miyake, F., Olsen, J., Reinig, F., Sakamoto, M., Sookdeo, A., Talamo, S., 2020. The IntCal20 northern hemisphere radiocarbon age calibration curve (0-55 cal kBP). Radiocarbon 62, 725–757. https://doi.org/10.1017/RDC.2020.41.
Reinig, F., Wacker, L., Jöris, O., Oppenheimer, C., Guidobaldi, G., Nievergelt, D., Adolphi, F., Cherubini, P., Engels, S., Esper, J., Land, A., Lane, C., Pfanz, H., Remmele, S., Sigl, M., Sookdeo, A., Büntgen, U., 2021. Precise date for the Laacher See eruption synchronizes the younger Dryas. Nature 595, 66–69. https://doi.org/10.1038/s41586-021-03608-x.
Reuther, A.U., Urdea, P., Geiger, C., Ivy-Ochs, S., Niller, H.P., Kubik, P.W., Heine, K., 2007. Late pleistocene glacial chronology of the Pietrele valley, Retezat mountains, southern Carpathians constrained by 10Be exposure ages and pedological investigations. Quat. Int. 164 (165), 151–169. https://doi.org/10.1016/j.quaint.2006.10.011.
Ruszkiczay-Rüdiger, Z., Kern, Z., Urdea, P., Braucher, R., Madarász, B., Schimmelpfennig, I., 2016. Revised deglaciation history of the Pietrele–Stânișoara glacial complex, Retezat Mts, southern Carpathians, Romania. Quat. Int. 415, 216–229.
Satow, C., Tomlinson, E.L., Grant, K.M., Albert, P.G., Smith, V.C., Manning, C.J., Ottolini, L., Wulf, S., Rohling, E.J., Lowe, J.J., Blockley, S.P.E., Menzies, M.A., 2015. A new contribution to the late quaternary tephrostratigraphy of the mediterranean: Aegean Sea core LC21. Quat. Sci. Rev. 117, 96–112. https://doi.org/10.1016/j.quascirev.2015.04.005.
Scaillet, S., Vita-Scaillet, G., Rotolo, S.G., 2013. Millennial-scale phase relationships between ice-core and Mediterranean marine records: insights from high-precision 40Ar/39Ar dating of the Green Tuff of Pantelleria, Sicily Strait. Quat. Sci. Rev. 78, 141–154. https://doi.org/10.1016/j.quascirev.2013.08.008.
Schmidt, R., van den Bogaard, C., Merkt, J., Müller, J., 2002. A new Lateglacial chronostratigraphic tephra marker for the south-eastern Alps: the Neapolitan Yellow Tuff (NYT) in Längsee (Austria) in the context of a regional biostratigraphy and palaeoclimate. Quat. Int. 88, 45–56. https://doi.org/10.1016/S1040-6182(01)00072-6.
Schmincke, H.U., Sumita, M., 2014. Impact of volcanism on the evolution of Lake Van (eastern Anatolia) III: Periodic (Nemrut) vs. episodic (Süphan) explosive eruptions and climate forcing reflected in a tephra gap between ca. 14 ka and ca. 30 ka. J. Volcanol. Geoth. Res. 285, 195–213. https://doi.org/10.1016/j.jvolgeores.2014.08.015.
Siani, G., Sulpizio, R., Paterne, M., Sbrana, A., 2004. Tephrostratigraphy study for the last 18,000 14C years in a deep-sea sediment sequence for the South Adriatic. Quat. Sci. Rev. 23, 2485–2500. https://doi.org/10.1016/j.quascirev.2004.06.004.
Sigvaldason, G.E., 2002. Volcanic and tectonic processes coinciding with glaciation and crustal rebound: an early Holocene rhyolitic eruption in the Dyngjufjöll volcanic centre and the formation of the Askja caldera, north Iceland. Bull. Volcanol. 64, 192–205. https://doi.org/10.1007/s00445-002-0204-7.
Smith, V.C., Isaia, R., Pearce, N.J.G., 2011. Tephrostratigraphy and glass compositions of post-15 kyr Campi Flegrei eruptions: implications for eruption history and chronostratigraphic markers. Quat. Sci. Rev. 30, 3638–3660. https://doi.org/10.1016/j.quascirev.2011.07.012.
Speranza, F., Landi, P., D'Ajello Caracciolo, F., Pignatelli, A., 2010. Paleomagnetic dating of the most recent silicic eruptive activity at Pantelleria (Strait of Sicily). Bull. Volcanol. 72, 847–858. https://doi.org/10.1007/s00445-010-0368-5.

Steffensen, J.P., Andersen, K.K., Bigler, M., Clausen, H.B., Dahl-Jensen, D., Fischer, H., Goto-Azuma, K., Hansson, M., Johnsen, S.J., Jouzel, J., Masson-Delmotte, V., Popp, T., Rasmussen, S.O., Rothlisberger, R., Ruth, U., Stauffer, B., Siggaard-Andersen, M.-L., Sveinbjornsdottir, A.E., Svensson, A., White, J.W.C., 2008. High-resolution Greenland ice core data show abrupt climate change Happens in Few Years. Science 321 (1979), 680–684. https://doi.org/10.1126/science.1157707.

Stevenson, J.A., Loughlin, S.C., Font, A., Fuller, G.W., MacLeod, A., Oliver, I.W., Jackson, B., Horwell, C.J., Thordarson, T., Dawson, I., 2013. UK monitoring and deposition of tephra from the May 2011 eruption of Grímsvötn, Iceland. Journal of Applied Volcanology 2, 3. https://doi.org/10.1186/2191-5040-2-3.

Striberger, J., Björck, S., Holmgren, S., Hamerlík, L., 2012. The sediments of Lake Lögurinn – a unique proxy record of Holocene glacial meltwater variability in eastern Iceland. Quat. Sci. Rev. 38, 76–88. https://doi.org/10.1016/j.quascirev.2012.02.001.

Sun, S. -s., McDonough, W.F., 1989. Chemical and isotopic systematics of oceanic basalts: implications for mantle composition and processes. Geological Society, London, Special Publications 42, 313–345. https://doi.org/10.1144/GSL.SP.1989.042.01.19.

Szabó, Z., Heiri, O., Wulf, S., Darabos, G., Pálfi, I., Molnár, M., Korponai, J., Magyari, E., 2023. Warm younger Dryas summer temperatures in the south Carpathians. In: INQUA Conference, 14th -20th July 2023. Rome, Italy.

Tamburrino, S., Insinga, D.D., Sprovieri, M., Petrosino, P., Tiepolo, M., 2012. Major and trace element characterization of tephra layers offshore Pantelleria Island: insights into the last 200 ka of volcanic activity and contribution to the Mediterranean tephrochronology. J. Quat. Sci. 27, 129–140. https://doi.org/10.1002/jqs.1504.

Thornalley, D.J.R., McCave, I.N., Elderfield, H., 2011. Tephra in deglacial ocean sediments south of Iceland: stratigraphy, geochemistry and oceanic reservoir ages. J. Quat. Sci. 26, 190–198. https://doi.org/10.1002/jqs.1442.

Timms, R.G.O., Matthews, I.P., Lowe, J.J., Palmer, A.P., Weston, D.J., MacLeod, A., Blockley, S.P.E., 2019. Establishing tephrostratigraphic frameworks to aid the study of abrupt climatic and glacial transitions: a case study of the Last Glacial-Interglacial Transition in the British Isles (c. 16-8 ka BP). Earth Sci. Rev. https://doi.org/10.1016/j.earscirev.2019.01.003.

Timms, R.G.O., Matthews, I.P., Palmer, A.P., Candy, I., 2018. Toward a tephrostratigraphic framework for the British Isles: a last glacial to interglacial transition (LGIT c. 16-8 ka) case study from Crudale meadow, Orkney. Quat. Geochronol. 46, 28–44. https://doi.org/10.1016/j.quageo.2018.03.008.

Timms, R.G.O., Matthews, I.P., Palmer, A.P., Candy, I., Abel, L., 2017. A high-resolution tephrostratigraphy from Quoyloo Meadow, Orkney, Scotland: implications for the tephrostratigraphy of NW Europe during the last glacial-interglacial transition. Quat. Geochronol. 40, 67–81. https://doi.org/10.1016/j.quageo.2016.06.004.

Tomlinson, Emma L., Arienzo, I., Civetta, L., Wulf, S., Smith, V.C., Hardiman, M., Lane, C.S., Carandente, A., Orsi, G., Rosi, M., Müller, W., Menzies, M.A., 2012b. Geochemistry of the Phlegraean Fields (Italy) proximal sources for major Mediterranean tephras: implications for the dispersal of Plinian and co-ignimbritic components of explosive eruptions. Geochem. Cosmochim. Acta 93, 102–128. https://doi.org/10.1016/j.gca.2012.05.043.

Tomlinson, E.L., Kinvig, H.S., Smith, V.C., Blundy, J.D., Gottsmann, J., Müller, W., Menzies, M.A., 2012a. The Upper and Lower Nisyros Pumices: Revisions to the Mediterranean tephrostratigraphic record based on micron-beam glass geochemistry. J. Volcanol. Geoth. Res. 243 (244), 69–80. https://doi.org/10.1016/j.jvolgeores.2012.07.004.

Tomlinson, E.L., Smith, V.C., Albert, P.G., Aydar, E., Civetta, L., Cioni, R., Çubukçu, E., Gertisser, R., Isaia, R., Menzies, M.A., Orsi, G., Rosi, M., Zanchetta, G., 2015. The major and trace element glass compositions of the productive Mediterranean volcanic sources: Tools for correlating distal tephra layers in and around Europe. Quat. Sci. Rev. 118, 48–66. https://doi.org/10.1016/j.quascirev.2014.10.028.

Tomlinson, E.L., Thordarson, T., Müller, W., Thirlwall, M., Menzies, M.A., 2010. Microanalysis of tephra by LA-ICP-MS - strategies, advantages and limitations assessed using the Thorsmörk ignimbrite (Southern Iceland). Chem. Geol. 279, 73–89. https://doi.org/10.1016/j.chemgeo.2010.09.013.

Tryon, C.A., Logan, M.A.V., Mouralis, D., Kuhn, S., Slimak, L., Balkan-Atli, N., 2009. Building a tephrostratigraphic framework for the paleolithic of central Anatolia, Turkey. J. Archaeol. Sci. 36, 637–652. https://doi.org/10.1016/j.jas.2008.10.006.

Turney, C.S.M., 1998. Extraction of rhyolitic component of Vedde microtephra from minerogenic lake sediments. J. Paleolimnol. 19, 199–206. https://doi.org/10.1023/A:1007926322026.

Turney, C.S.M., Harkness, D.D., Lowe, J.J., 1997. The use of microtephra horizons to correlate Late-glacial lake sediment successions in Scotland. J. Quat. Sci. 12, 525–531. https://doi.org/10.1002/(SICI)1099-1417(199711/12)12:6<525::AID-JQS347>3.0.CO;2-M.

Turney, C.S.M., van den Burg, K., Wastegård, S., Davies, S.M., Whitehouse, N.J., Pilcher, J.R., Callaghan, C., 2006. North European last glacial-interglacial transition (LGIT; 15-9 ka) tephrochronology: extended limits and new events. J. Quat. Sci. 21, 335–345. https://doi.org/10.1002/jqs.990.

Urdea, P., 2004. The pleistocene glaciation of the Romanian Carpathians. In: Quaternary Glaciations-Extent and Chronology, pp. 301–308. https://doi.org/10.1016/S1571-0866(04)80080-0.

van der Bilt, W.G.M., Lane, C.S., Bakke, J., 2017. Ultra-distal Kamchatkan ash on Arctic Svalbard: towards hemispheric cryptotephra correlation. Quat. Sci. Rev. 164, 230–235. https://doi.org/10.1016/j.quascirev.2017.04.007.

Veres, D., Lane, C.S., Timar-Gabor, A., Hambach, U., Constantin, D., Szakács, A., Fülling, A., Onac, B.P., 2013. The Campanian Ignimbrite/Y5 tephra layer - a regional stratigraphic marker for Isotope Stage 3 deposits in the Lower Danube region, Romania. Quat. Int. 293, 22–33. https://doi.org/10.1016/j.quaint.2012.02.042.

Vincze, I., Orbán, I., Birks, H.H., Pál, I., Finsinger, W., Hubay, K., Marinova, E., Jakab, G., Braun, M., Biró, T., Tóth, M., Dănău, C., Ferencz, I.V., Magyari, E.K., 2017. Holocene treeline and timberline changes in the South Carpathians (Romania): climatic and anthropogenic drivers on the southern slopes of the Retezat Mountains. Holocene 27, 1613–1630. https://doi.org/10.1177/0959683617702227.

Vogel, H., Zanchetta, G., Sulpizio, R., Wagner, B., Nowaczyk, N., 2010. A tephrostratigraphic record for the last glacial-interglacial cycle from Lake Ohrid, Albania and Macedonia. J. Quat. Sci. 25, 320–338. https://doi.org/10.1002/jqs.1311.

Wastegård, S., 1998. Deglaciation chronology and marine environments in southwestern Sweden. Boreas 27, 178–194. https://doi.org/10.1111/j.1502-3885.1998.tb00877.x.

Wastegård, S., Gudmundsdóttir, E.R., Lind, E.M., Timms, R.G.O., Björck, S., Hannon, G. E., Olsen, J., Rundgren, M., 2018. Towards a Holocene tephrochronology for the Faroe Islands, north atlantic. Quat. Sci. Rev. 195, 195–214. https://doi.org/10.1016/j.quascirev.2018.07.024.

Wastegård, S., Turney, C.S.M., Lowe, J.J., Roberts, S.J., 2000. New discoveries of the Vedde ash in southern Sweden and Scotland. Boreas 29, 72–78. https://doi.org/10.1111/j.1502-3885.2000.tb01201.x.

Wastegård, S., Wohlfarth, B., Subetto, D.A., Sapelko, T.V., 2000. Extending the known distribution of the younger Dryas Vedde ash into northwestern Russia. J. Quat. Sci. 15, 581–586.

Watson, E.J., Swindles, G.T., Savov, I.P., Lawson, I.T., Connor, C.B., Wilson, J.A., 2017. Estimating the frequency of volcanic ash clouds over northern Europe. Earth Planet Sci. Lett. 460, 41–49. https://doi.org/10.1016/j.epsl.2016.11.054.

Watt, S.F.L., Gilbert, J.S., Folch, A., Phillips, J.C., Cai, X.M., 2015. An example of enhanced tephra deposition driven by topographically induced atmospheric turbulence. Bull. Volcanol. 77 https://doi.org/10.1007/s00445-015-0927-x.

Wohlfarth, B., Blaauw, M., Davies, S.M., Andersson, M., Wastegård, S., Hormes, A., Possnert, G., 2006. Constraining the age of Lateglacial and early Holocene pollen zones and tephra horizons in southern Sweden with Bayesian probability methods. J. Quat. Sci. 21, 321–334. https://doi.org/10.1002/jqs.996.

Wohlfarth, B., Luoto, T.P., Muschitiello, F., Väliranta, M., Björck, S., Davies, S.M., Kylander, M., Ljung, K., Reimer, P.J., Smittenberg, R.H., 2018. Climate and environment in southwest Sweden 15.5–11.3 cal. ka BP. Boreas 47, 687–710. https://doi.org/10.1111/bor.12310.

Wulf, S., Dräger, N., Ott, F., Serb, J., Appelt, O., Gudmundsdóttir, E., van den Bogaard, C., Słowiński, M., Błaszkiewicz, M., Brauer, A., 2016a. Holocene tephrostratigraphy of varved sediment records from lakes Tiefer See (NE Germany) and Czechowskie (N Poland). Quat. Sci. Rev. 132, 1–14. https://doi.org/10.1016/j.quascirev.2015.11.007.

Wulf, S., Fedorowicz, S., Veres, D., Łanczont, M., Karátson, D., Gertisser, R., Bormann, M., Magyari, E., Appelt, O., Hambach, U., Gozhyk, P.F., 2016b. The 'Roxolany tephra' (Ukraine) – new evidence for an origin from Ciomadul volcano, east Carpathians. J. Quat. Sci. 31, 565–576. https://doi.org/10.1002/jqs.2879.

Wulf, S., Kraml, M., Brauer, A., Keller, J., Negendank, J.F.W., 2004. Tephrochronology of the 100ka lacustrine sediment record of Lago Grande di Monticchio (southern Italy). Quat. Int. 122, 7–30. https://doi.org/10.1016/j.quaint.2004.01.028.

Wulf, S., Kraml, M., Keller, J., 2008. Towards a detailed distal tephrostratigraphy in the Central Mediterranean: the last 20,000 yrs record of Lago Grande di Monticchio. J. Volcanol. Geoth. Res. 177, 118–132. https://doi.org/10.1016/j.jvolgeores.2007.10.009.

Yılmaz, Y., Güner, Y., Şaroğlu, F., 1998. Geology of the quaternary volcanic centres of the east Anatolia. J. Volcanol. Geoth. Res. 85, 173–210. https://doi.org/10.1016/S0377-0273(98)00055-9.

Zanchetta, G., Sulpizio, R., Roberts, N., Cioni, R., Eastwood, W.J., Siani, G., Caron, B., Paterne, M., Santacroce, R., 2011. Tephrostratigraphy, chronology and climatic events of the Mediterranean basin during the Holocene: an overview. Holocene 21, 33–52. https://doi.org/10.1177/0959683610377531.